The Large Scale Structure of the Cosmic Microwave Background

E. B. Rørnes*
Institute of Physics, University of Oslo,
0371 Oslo, Norway
(Dated: May 4, 2024)

In this paper we consider the large scale structure of the universe and the Cosmic Microwave Background (CMB) fluctuations...

INTRODUCTION

This project was built on the template provided from [1] which already contains a large part of the structure behind the numerical parts of the project. In the entire paper the subscript 0 denotes today's values whilst a superscript 0 represents an equilibrium. Note that throughout the article there are many switches between natural units where $c = \hbar = k_b = 1$ and SI units for . (not a final introduction)

1. MILESTONE I

In this section we consider the evolution of the uniform background of the universe in the Lambda-Cold-Dark-Matter (ΛCDM) model which is considered to be the present day standard model of cosmology. The main goal of this section is to solve the unperturbed background evolution of the universe by using known cosmological parameters supplied by [2] and comparing this to observational supernova data from [3].

1.1. Theory

1.1.1. Friedmann-Lemaître-Robertson-Walker

In this milestone we approximate the universe to be completely isotropic and homogeneous over all scales. For large scales this has been shown to be a reasonable assumption from observations of the CMB power spectra [4]. The universe must then satisfy a maximally symmetric metric. With some symmetry arguments, we arrive at an exact solution for the metric called the Friedmann-Lemaître-Robertson-Walker (FLRW) metric. In flat space, $k = 0$, and Cartesian coordinates it is given by:

$$g_{\mu\nu} = \text{diag}\left[-1, a^2(t), a^2(t), a^2(t)\right],$$

where $a(t)$ is the scale factor, defined to be 1 today, and we are using the mostly plus metric signature $(-,+,+,+)$.

To make use of the line element above we consider the Einstein field equations (EFE):

$$G_{\mu\nu} + \Lambda g_{\mu\nu} = 8\pi G T_{\mu\nu}, \tag{1}$$

With the isotropy requirement, any stress-energy tensors which we will consider must be invariant under spatial rotations. To consider the general allowed form of the stress-energy tensor we decompose it as such:

$$T_{\mu\nu}(x) = \begin{bmatrix} T_{00}(x) & T_{0i}(x) \\ T_{0i}(x) & \sigma_{ij}(x) \end{bmatrix},$$

As usual, the $T_{00} = \rho$ component is to be interpreted as the energy density in a non-boosted frame. The requirement of homogeneity then imposes that one should not have any energy flux, as such finds $T_{0i} = 0$. The isotropy requirement imposes that the matrix σ must satisfy $R^T\sigma(x)R = \sigma(x)$ for all x and rotation matrices R. The latter then implies that $[R, \sigma(x)] = 0$. As the generators of the $SO(3)$ group form an algebra, Schurs' Lemma then states that this is satisfied iff $\sigma(x) \propto I \implies \sigma(x) = p(x)I$ for some function $p(x)$. Furthermore the homogeneity requirement imposes translation invariance, meaning that $p(x) = p(x + x_0)$. These requirements, a comoving observer, i.e. an observer in the rest frame of the universe, then implies that we may uniquely describe the universe as a perfect liquid with:

$$T_{\mu\nu} = (\rho + p)u_\mu u_\nu + g_{\mu\nu}p.$$

where p is the pressure. As such, from the FRWL metric and the EFE one can derive the **Friedmann equations**:

$$\left(\frac{\dot{a}}{a}\right)^2 \equiv H^2 = \frac{8\pi G}{3}\rho, \tag{2}$$

$$\frac{\ddot{a}}{a} = -\frac{4\pi G}{3}(\rho + 3p), \tag{3}$$

where ρ and p are, as explained, the energy density and pressure respectively for a perfect liquid.

1.1.2. ΛCDM Model

The ΛCDM model is derived by assuming; that we have some family of weakly interacting massive particles (WIMPs) which we call cold-dark-matter (CDM) and a cosmological constant, Λ, which accounts for the present

* e.b.rornes@fys.uio.no

day acceleration of the universe, which will be the dark energy in this article. The name CDM comes from assuming that they are massive enough to not be relativistic and hence cold. The first Friedmann equation (2) can be rewritten such that the time dependence of the Hubble factor $H \equiv \dot{a}/a$ is given by:

$$H^2 = H_0^2 \sum_i \Omega_{i0} a^{-3(1+\omega_i)}, \tag{4}$$

where $\omega_i \equiv p_i/\rho_i$ is the equation of state for the i-th particle type, $\Omega_i \equiv \rho_i/\rho_C$ is the relative energy density of the i-th particle type, ρ_i is the energy density corresponding to the i-th particle type and $\sum_i \rho_i = \rho_C$ is the critical energy density required to have a flat universe which we observe today [2]. We have that $\omega_{\mathrm{B}} = 0, \omega_{\mathrm{R}} = 1/3$ and $\omega_\Lambda = -1$ for baryons, relativistic particles (photons and massless neutrinos) and dark energy (DE) respectively. Simply plugging in the various particle types in (4) we have:

$$\begin{gathered} H = H_0 \sqrt{\Omega_{\mathrm{M0}} a^{-3} + \Omega_{\mathrm{R0}} a^{-4} + \Omega_{\mathrm{K0}} a^{-2} + \Omega_{\Lambda 0}}, \\ \Omega_{\mathrm{M0}} \equiv \Omega_{B0} + \Omega_{\mathrm{CDM0}}, \quad \Omega_{\mathrm{R0}} \equiv \Omega_{\gamma 0} + \Omega_{\nu 0}, \end{gathered} \tag{5}$$

where $\Omega_{B0}, \Omega_{\mathrm{CDM0}}, \Omega_{\gamma 0}, \Omega_{\nu 0}$ and $\Omega_{\Lambda 0}$ are then the present day relative densities of baryonic matter (electrons & protons), cold dark matter, radiation, neutrinos and dark energy respectively. The term $\Omega_{\mathrm{K0}} = -kc^2/H_0$ denotes the curvature of the universe and encapsulates how said curvature affects expansion rates and energy densities. With the requirement for a flat universe we have that $\sum_i \Omega_i = 1$ where i refers to all non-curvature energy types. Since Ω_{B}, Ω_{CDM} and Ω_γ, Ω_ν give the same contribution to the time evolution of the Hubble parameter, we will often bundle these together as "matter" and "radiation" (or "relativistic") particles respectively as was done in (5).

The other Friedmann equation (3), together with each particles equation of state, is then used to describe how each component evolves with time:

$$\begin{aligned} \Omega_{\mathrm{B}}(a) &= \frac{\Omega_{\mathrm{B0}}}{a\mathcal{H}^2/H_0^2}, \quad \Omega_{\mathrm{CDM}}(a) = \frac{\Omega_{\mathrm{CDM0}}}{a\mathcal{H}^2/H_0^2}, \\ \Omega_\gamma(a) &= \frac{\Omega_{\gamma 0}}{a^2\mathcal{H}^2/H_0^2}, \qquad \Omega_\nu(a) = \frac{\Omega_{\nu 0}}{a^2\mathcal{H}^2/H_0^2}, \\ \Omega_{\mathrm{K}}(a) &= \frac{\Omega_{\mathrm{K0}}}{\mathcal{H}^2/H_0^2}, \qquad \Omega_\Lambda(a) = \frac{\Omega_{\Lambda 0}}{H^2/H_0^2}, \end{aligned} \tag{6}$$

where $\mathcal{H} \equiv aH$ is the **conformal Hubble factor**. Two of the six density parameters follow from the observed temperature of the CMB and are given by:

$$\Omega_{\gamma 0} = \frac{8\pi^3 G}{45 H_0^2} \frac{(k_B T_{\mathrm{CMB0}})^4}{\hbar^3 c^5}, \tag{7}$$

$$\Omega_{\nu 0} = \Omega_{\gamma 0} N_{\mathrm{eff}} \cdot \frac{7}{8} \left(\frac{4}{11}\right)^{4/3}, \tag{8}$$

where T_{CMB0} is the temperature of CMB photons today and $N_{\mathrm{eff}} = 3.046$ is the effective number of massless neutrinos. [2]

The ΛCDM model is then fully determined by these cosmological observables which come from 2018 Planck [2]:

$$\begin{aligned} \frac{H_0\,\mathrm{Mpc}}{100\,\mathrm{km/s}} \equiv h = 0.67, &\qquad N_{\mathrm{eff}} = 3.046, \\ \Omega_{\mathrm{B0}} = 0.05, &\qquad \Omega_{\mathrm{CDM0}} = 0.267, \\ \Omega_{\mathrm{K0}} = 0.00, &\qquad T_{\mathrm{CMB0}} = 2.7255. \end{aligned} \tag{9}$$

1.1.3. Time and Distance Measurements in Cosmology

Since the expansion of the universe is strictly positive w.r.t. time, the scale factor $a(t)$ is an injective function and can thus be used as a time measurement. In this paper we will, for computational purposes, be using the variable $x \equiv \ln(a) \implies a = e^x$.

Again, due to the expansion of the universe, one can also measure how much the wavelength of a photon released at initial time t_i has stretched before it reaches us at final time t_f, commonly known as the **redshift**:

$$z = e^{x(t_f) - x(t_i)} - 1.$$

A derivation can be found in [5]. Since we are mainly interested in the redshift w.r.t. today then $x(t_f) = 0$. Thus the formula which will be used in this article is $z = e^{-x(t_i)} - 1$.

Further we consider the **horizon**, i.e. the "distance" massless particles may have travelled since the big bang. Since the universe is expanding, this will be appreciably larger than ct. Considering a time t_1, light would have travelled a distance $d_1 > ct_1$. We can then consider what t_1 must be such that this becomes an equality. For this we define the **conformal time** $d\eta = dt/a$ (or conformal distance with the appropriate insertion of c) which can be rewritten as $\eta(t) \equiv \int_0^t \frac{c}{a} dt'$ and we get the differential equation:

$$\frac{d\eta}{dx} = \frac{c}{\mathcal{H}}, \tag{10}$$

along with the initial condition $\eta(-\infty) = 0$, which can be solved analytically in the radiation dominated era. We will then use the analytical solution to approximate that at some very early time, x_{start} such that we have the new initial condition $\eta(x_{\mathrm{start}}) = c/\mathcal{H}(x_{\mathrm{start}})$ where we will solve onwards numerically.

A useful distance measure is the **comoving distance** χ which is derived by the FLRW metric:

$$\chi = \int_{t_i}^{t_0} dt \frac{c}{a} = \int_1^a da' \frac{c}{a'^2 H} = \int_0^z dz' \frac{c}{H} = \eta - \eta_0.$$

Considering a light-like path with the FLRW metric in

curved space one arrives at the **proper distance** r:

$$r = \begin{cases} \chi \frac{\sin\left(\sqrt{|\Omega_{\rm K0}|}H_0\chi/c\right)}{\sqrt{|\Omega_{\rm K0}|}H_0\chi/c}, & \Omega_{\rm K0} < 0 \text{ "Closed"} \\ \chi, & \Omega_{\rm K0} = 0 \text{ "Flat"} \\ \chi \frac{\sinh\left(\sqrt{|\Omega_{\rm K0}|}H_0\chi/c\right)}{\sqrt{|\Omega_{\rm K0}|}H_0\chi/c}, & \Omega_{\rm K0} > 0 \text{ "Open"} \end{cases}.$$

We then consider the angular **diameter distance** $d_A = \Delta s/\Delta\theta$ where Δs is the objects physical size and $\Delta\theta$ its angular size as viewed from Earth. Once again from the FRLW metric, now in spherical coordinates:

$$ds^2 = -c^2dt^2 + a^2(dr^2 + r^2d\theta^2 + \sin^2\theta d\phi^2),$$

one can find that this can be expressed in terms of our cosmological parameters as $d_A = ar$. The **luminosity distance** d_L is defined from $d_L = \sqrt{\frac{L}{4\pi F}}$ where L is the intrinsic luminosity and F is the measured flux. As implied by its name, this quantity is related to d_A by $d_L = d_A/a^2 = r/a$.

At last we consider the **cosmic time** t in our x coordinate:

$$t(x) = \int_0^a \frac{da}{aH} = \int_{-\infty}^0 \frac{dx}{H(x)}.$$

From this we get to the ODE:

$$\frac{dt}{dx} = \frac{1}{H}, \tag{11}$$

with the initial condition $t(-\infty) = 0$. This initial condition states that cosmic time begins once the big bang happened. As before, we make an analytical approximation which gives us the initial condition $t(x_{\rm start}) = \frac{1}{2H(x_{\rm start})}$ and solved numerically from here.

1.1.4. Markov-Chain Monte Carlo Method

In this milestone one of the major computational method which will be used is the Markov Chain Monte Carlo (MCMC) method. The particular algorithm we use is the Metropolis algorithm which generates a Markov chain, where in each step, the chain corresponds to a proposed set of model parameters, which in our case are $h, \Omega_{\rm M0}$ and $\Omega_{\rm K0}$. These parameters are sampled from a probability distribution guided by certain priors, i.e. accepted ranges, where data outside of these priors are omitted. The algorithm then eventually converges to the posterior distribution of the parameters given the observed data. This can then be used to constrain the cosmological parameters, in which we decide to focus on $h, \Omega_{\rm CDM0}$ and $\Omega_{\rm M0}$. A χ^2-test is then done by the assumption that the measurements are Gaussian distributed and uncorrelated between different redshift. The likelihood function is then given by $L \propto e^{-\chi^2/2}$ where:

$$\chi^2(h, \Omega_{\rm M0}, \Omega_{\rm K0}) = \sum_{i=1}^{N} [d_L(z_i, h, \Omega_{\rm M0}, \Omega_{\rm K0}) - d_L^{\rm obs}]^2/\sigma_i^2.$$

Here σ_i is the standard deviation for the i-th data point and N is the total number of data points. The set of parameters with the highest likelihood is our best-fit model, which also happen to be the values which minimize χ^2. To check that this best-fit is in fact a good fit one can consider a set of data points which all lie exactly 1σ away from the observed values. As such the expression in the sum simply reduces to 1. Thus when summing over N terms equal to 1 we would have that $\chi^2/N = 1$. Hence we will consider a best-fit to be a good fit if $\chi^2 \sim N$. For the case when $\chi^2 \ll N$ then we over-fit the model, meaning we may be capturing random noise and fluctuations in the data, whilst if $\chi^2 \gg N$ then we simply have a bad correspondence with the data and/or underlying assumptions (such as the assumption that the measurements are Gaussian).

1.2. Implementation details

1.2.1. Solving the ODEs

To implement some numerical tools to solve for the background we first implement the data from (9) and computed the derived quantities $\Omega_{\gamma 0}$ and $\Omega_{\nu 0}$ with (7,8), and $\Omega_{\Lambda 0} = 1 - \Omega_{\rm rest0}$ where "rest" refers to all the other Ω_i.

Next we implemented an ordinary differential equation (ODE) solver to solve the ODEs for $\eta(x)$ and $t(x)$. This was done by first setting up the respective differential equation (10,11) with its corresponding initial condition, then an ODE solver was used to get a result which was then splined. The ODE solver and splining programs were already provided in the template.

Further we computed $H(x)$ from (5) which was used together with the various relations from the theory section to compute $\mathcal{H}, \frac{d\mathcal{H}}{dx}, \frac{d^2\mathcal{H}}{dx^2}, \Omega_i, r, d_A, d_L, \chi$ and $T_{\rm CMB}$ all as a function of our time variable x. Note that the expressions for $\frac{d\mathcal{H}}{dx}$ and $\frac{d^2\mathcal{H}}{dx^2}$ were found analytically from 5. The calculated data was then written to data files to be analyzed in Python.

1.2.2. MCMC fit

We then compared our numerical data for the luminosity distance d_L to observational data from [3], containing $N = 31$ data points, by performing an MCMC fit. The upper and lower priors which were used are $\{1.5, 1, 1\}$ and $\{0.5, 0, -1\}$ for $h, \Omega_{\rm M}$ and $\Omega_{\rm K}$ respectively. The algorithm then computes an initial χ^2 with some randomly generated parameters. It repeats this process and checks whether the new $\chi^2_{\rm new}$ is less than the old $\chi^2_{\rm old}$. If this is the case then it accepts this sample and starts again. However if this previous test is not the case we then perform a random check $e^{-(\chi^2_{\rm new} - \chi^2_{\rm old})/2} > u$ where u is number drawn from a uniform distribution in the interval $[0, 1]$. If it passes this test then $\chi^2_{\rm new}$ is accepted and the

process carries on. This additional test is the main part of the Metropolis algorithm and is done to capture the full posterior probability distribution function (PDF) of the various parameters. As before, the data was printed to a data file and imported to Python.

1.2.3. Python

x-values corresponding to radiation-matter- and matter-DE-equality were found by finding running a script over the data to find where the absolute value of the difference $|\Omega_i - \Omega_j| = 0$. In reality they were never quite 0 due to running over a discrete index, thus we simply set some low threshold, e.g. $5 \cdot 10^{-5}$. To find when the universe accelerates we note that:

$$\mathcal{H} = \frac{\dot{a}}{a}a = \dot{a} \implies \frac{d\mathcal{H}}{dx} = \frac{d\mathcal{H}}{dt}\frac{dt}{dx} = \ddot{a}\frac{dt}{dx},$$

and from (11) we then have:

$$\frac{d\mathcal{H}}{dx} \equiv \mathcal{H}' = \frac{\ddot{a}}{H}.$$

Since H is strictly positive we can then look at when $\mathcal{H}'$ changes from negative to positive. So again a Python script which runs over the indices of $\mathcal{H}$ were used to find which x-values this sign change happened, which corresponds to where the universe began to accelerate.

The MCMC-fit was then analyzed and a scatterplot in the $\Omega_\Lambda\Omega_\mathrm{M}$-plane was created with the $(1\sigma, 2\sigma)$ confidence regions $\chi^2 - \chi^2_\mathrm{min} < (3.53, 8.02)$ respectively. These particular values were found from common χ^2 distribution tables with $k = 3$ degrees of freedom. A histogram of the PDF from the accepted samples of h along with a Gaussian fit was along with a comparison of our theoretical d_L vs. the real supernova data were also plotted.

1.3. Tests of data

Before considering the results it is reasonable to conduct some sanity checks on the data to make sure everything was implemented correctly. To check that the data is consistent with the analytical expressions we consider the following quantities analytically in the different regimes:

$$\frac{\mathcal{H}'}{\mathcal{H}}, \quad \frac{1}{\mathcal{H}}\frac{d^2\mathcal{H}}{dx^2} \equiv \frac{\mathcal{H}''}{\mathcal{H}}, \quad \frac{1}{c}\eta\mathcal{H}.$$

1.3.1. $\mathcal{H}'$ and $\mathcal{H}''$

In the radiation dominated era where we approximate $\Omega_\mathrm{R} \approx 1 \implies \Omega_\mathrm{rest} \approx 0$. Then by using (5) we find:

$$H_\mathrm{R}(x) \approx H_0, \quad \mathcal{H}_\mathrm{R}(x) \approx H_0 e^{-x},$$
$$\frac{\mathcal{H}'_\mathrm{R}}{\mathcal{H}_\mathrm{R}} \approx -1, \qquad \frac{\mathcal{H}''_\mathrm{R}}{\mathcal{H}_\mathrm{R}} \approx 1,$$

and similarly using the approximations $\Omega_\mathrm{M} \approx 1$ and $\Omega_\Lambda \approx 1$ respectively, we get:

$$H_\mathrm{M}(x) \approx H_0 e^{x/2}, \qquad \mathcal{H}_\mathrm{M}(x) \approx H_0 e^{-x/2},$$
$$\frac{\mathcal{H}'_\mathrm{M}}{\mathcal{H}_\mathrm{M}} \approx -1/2, \qquad \frac{\mathcal{H}''_\mathrm{M}}{\mathcal{H}_\mathrm{M}} \approx 1/4,$$
$$H_\Lambda(x) \approx H_0, \qquad \mathcal{H}_\Lambda(x) \approx H_0 e^{x},$$
$$\frac{\mathcal{H}'_\Lambda}{\mathcal{H}_\Lambda} \approx \frac{\mathcal{H}''_\Lambda}{\mathcal{H}_\Lambda} \approx 1.$$

Plotting these assumptions with the data we have FIG. 1. We see that there is a reasonable agreement with the analytical approximations in the given regimes. As we will see in later, $\Omega_\mathrm{M} \approx 1$ is a relatively poor approximation compared to the others, hence larger a deviation is to be expected.

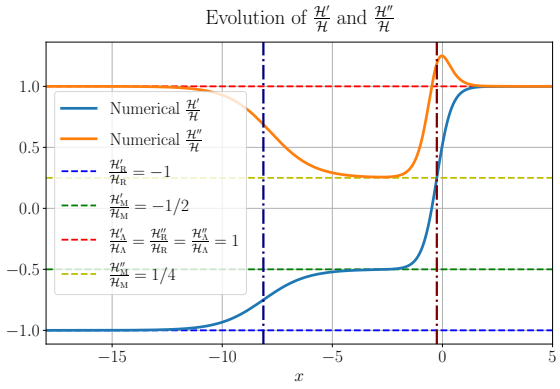

FIG. 1. $\mathcal{H}'/\mathcal{H}$ and $\mathcal{H}''/\mathcal{H}$ compared to analytical approximations in the various regimes where the left and right dash-dotted vertical lines signify radiation-matter equality and matter-dark energy equality respectively.

1.3.2. Conformal Time

Analytical approximations for the conformal time requires a little more effort. For the radiation dominated era we can solve (10) analytically:

$$\eta_\mathrm{R}(x) = \int_{-\infty}^{x} \frac{c}{\mathcal{H}_\mathrm{R}} dx' \approx \int_{-\infty}^{x} \frac{c}{H_0} e^{x'} dx' = \frac{c}{H_0} e^x.$$

Now we approximate this radiation dominated epoch to end abruptly at some time x_1 such that we can write the conformal time in the matter dominated epoch as:

$$\begin{aligned}\eta_\mathrm{M}(x) &\approx \eta_\mathrm{R}(x_1) + \int_{x_1}^{x} \frac{c}{\mathcal{H}_\mathrm{M}} dx' \\ &\approx \frac{c}{H_0}\left(e^{x_1} + \int_{x_1}^{x} e^{x'/2} dx'\right) \\ &= \frac{c}{H_0}(e^{x_1} - 2e^{x_1/2} + 2e^{x/2}).\end{aligned}$$

Again we assume that the matter dominated epoch ends abruptly at some time x_2 such that we can approximate:

$$\begin{aligned}\eta_\Lambda(x) &\approx \eta_\mathrm{M}(x_2) + \int_{x_2}^{\infty} \frac{c}{\mathcal{H}_\Lambda} dx' \\ &\approx \frac{c}{H_0}\left(e^{x_1} - 2e^{x_1/2} + 2e^{x_1/2} + \int_{x_2}^{x} e^{-x'} dx'\right) \\ &= \frac{c}{H_0}\left(e^{x_1} - 2e^{x_1/2} + 2e^{x_2/2} + e^{-x_2} - e^{-x}\right).\end{aligned}$$

Thus we find that for the various regimes we have:

$$\begin{aligned}&\eta_\mathrm{R}\mathcal{H}_\mathrm{R}/c \approx 1, \\ &\eta_\mathrm{M}\mathcal{H}_\mathrm{M}/c \approx (e^{x_1} - 2e^{x_2/2} + 2e^{x/2})e^{-x/2}, \\ &\eta_\Lambda\mathcal{H}_\Lambda/c \approx (e^{x_1} - 2e^{x_1/2} + 2e^{x_2/2} + e^{-x_2} - e^{-x})e^{x}.\end{aligned}$$

Using the x values corresponding to $\Omega_\mathrm{R} = \Omega_\mathrm{M}$ and $\Omega_\mathrm{M} = \Omega_\Lambda$ as the time where the respective epochs start and end we get the upper graph in FIG. 2. Clearly this approximation will be nothing close to exact due to the assumption that the epochs end abruptly when in reality the epoch's change continuously and relatively slowly. Since η depends on how long the previous epochs lasted we can see that this heavily affects the final epoch.

FIG. 2. Numerical $\eta\mathcal{H}/c$ compared to analytical approximations in the various regimes where epochs are approximated to abruptly once $\Omega_i = \Omega_j$.

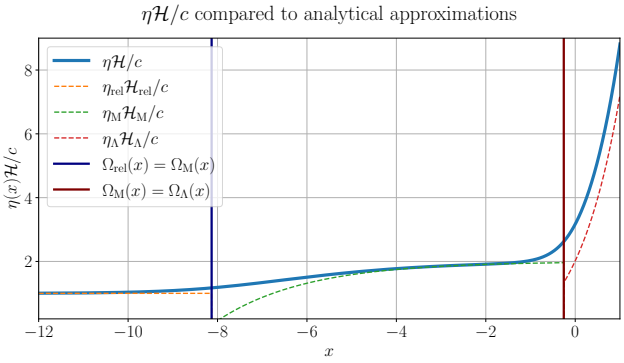

Overall the data seems to be consistent with the analytical expressions, even if the conformal time is a rather difficult parameter to define a robust approximation for.

1.4. Results

Now that the data has been stress tested to show that they are at least valid in certain regions we can go on to look at some of the results.

1.4.1. *Time Evolution of Cosmic Parameters*

We first consider the time evolution of the various relative energy densities Ω_i as a function of the scale factor $a(t)$ as given in FIG. 3.

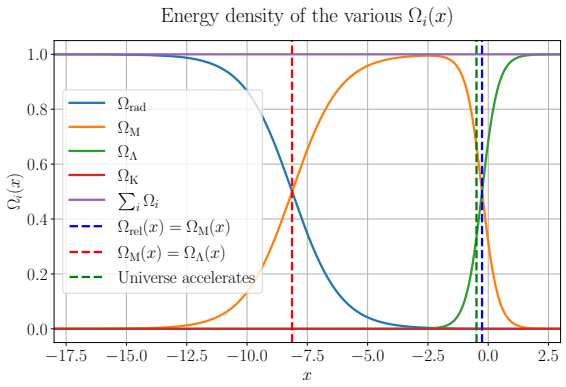

FIG. 3. Time evolution of the density parameters Ω_i as a function of the scale factor a.

Here we can clearly see the different regimes of the various quantities. The early universe is in a complete radiation domination at early times which implies that the universe expands $a(t) \propto t^{1/2}$. The universe then relatively slowly switches over to becoming matter dominated as time passes. For a short period of time we have complete matter domination, implying an expansion $a(t) \propto t^{2/3}$. Then dark energy starts to dominate at later times, causing the universe to begin to accelerate, until we get the known result of today where dark energy accounts for roughly 68% of the total energy in the universe today. It then further predicts that in the future, dark energy domination will continue to grow as time passes.

The time evolution of the conformal Hubble factor $\mathcal{H}(x)$, cosmic time $t(x)$ and conformal distance $\eta(x)/c$ is given in FIG. 4. The notable acceleration at later times in the $\mathcal{H}$ plot can be seen by when the derivative of $\mathcal{H}$ changes sign as mentioned previously. One can also see that this same phenomena affects both the cosmic time and conformal distance inversely at the same time. This is due to them both being inversely proportional to the conformal Hubble factor.

Next we consider the values of $x, z, t, \eta, \Omega_\mathrm{M}, \Omega_\Lambda$ and Ω_R at various important events. A summary of these events is given in TABLE I.

Here we can see that radiation-matter-equality happened roughly 51000 years after the big bang. Further, the universe begins to accelerate roughly 7.7 billion years after the big bang. One may notice that this happens $2\Omega_\Lambda \approx \Omega_\mathrm{M}$ and $\Omega_\mathrm{others} \approx 0$. We can check this analytically by considering these approximation. We have that $\Omega_\mathrm{tot} \approx 3\Omega_\Lambda$ and hence $\rho_\mathrm{tot} = 3\rho_\Lambda$. Further we have that $p_\mathrm{tot} = p_\Lambda + p_\mathrm{M} = p_\Lambda$ due to $p_\mathrm{M} = 0$ from its equation of state. Inserting this into the Friedman equation (3) with

TABLE I. Results for cosmological parameters at various important events from numerical data.

Event	x	$z(x)$	$t(x)$ [Gly]	$\eta(x)/c$ [Gly]	Ω_{M}	Ω_{Λ}	Ω_{Rel}
Radiation-Matter Equality	-8.132	3401	$5.106 \cdot 10^{-5}$	0.368	0.500	$2.737 \cdot 10^{-11}$	0.500
Universe Accelerates	-0.486	0.626	7.761	38.55	0.666	0.334	$3.183 \cdot 10^{-4}$
Matter-DE Equality	-0.256	0.292	10.38	42.33	0.500	0.500	$1.900 \cdot 10^{-4}$
Universe Today	0.000	0.000	13.86	46.29	0.317	0.683	$9.320 \cdot 10^{-5}$

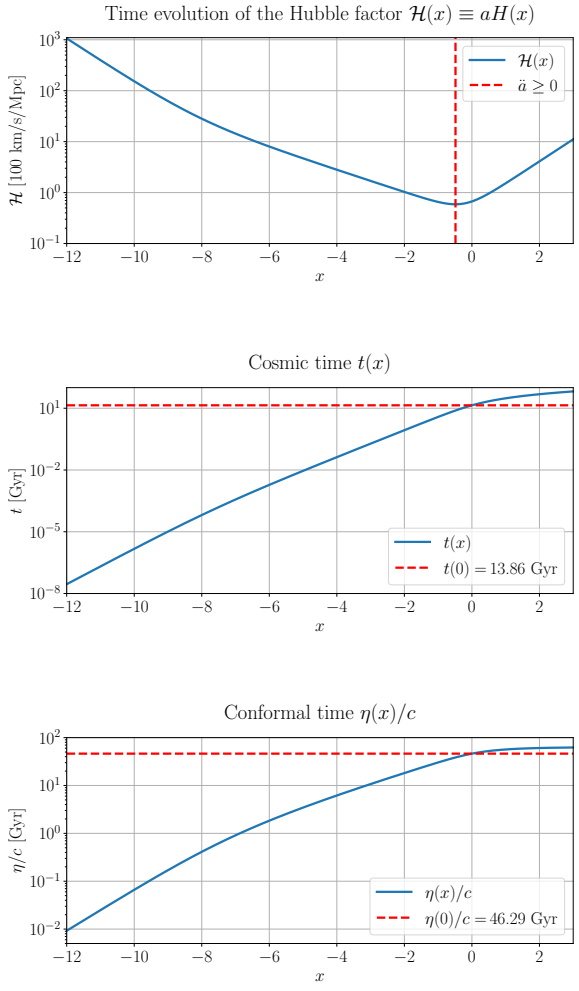

FIG. 4. Time evolution of the conformal Hubble factor $\mathcal{H}$, cosmic time t and conformal distance η/c as a function of x.

the relevant equation of state we get:

$$\frac{\ddot{a}}{a} \approx -\frac{4\pi G}{3}(3\rho_{\Lambda} + 3(p_{\Lambda} + p_{\mathrm{M}})) = -\frac{4\pi G}{3}(3\rho_{\Lambda} - 3\rho_{\Lambda}) = 0$$

Now, since a is strictly a positive number then, mathematically, all that remains to check whether this is not when deceleration starts or a terrace point. To ensure this one can just check some arbitrarily close points such as $\Omega_{\Lambda} = 1/3 \pm \epsilon$ and $\Omega_{\mathrm{M}} = 2/3 \mp \epsilon$ where ϵ is some tiny positive number.

Next in the table we have $t(x = 0)$ which corresponds to the age of the universe today. [2] estimates this to be 13.78 ± 0.20 Gly which is reasonably close to our value of 13.86 Gly. Similarly $\eta(x = 0)$ shows us the actual size of the observable universe today. [6] states the expected conformal distance of the universe is roughly 14 Gpc which corresponds to 45.7 Gly, again in reasonable agreement with the data.

1.4.2. Supernova Comparison

Further we compare our numerical data to data collected from supernova observations [3] by; comparing the luminosity distance is given in FIG. 5 and making a posterior probability distribution function (PDF) of the Hubble parameter H_0 in FIG. 6. We note that the found $\chi^2_{\mathrm{min}} = 29.3$ for the MCMC fit, which then yields that for the points accepted within the 1σ region follow $\chi^2 \sim N$ to a very good approximation, suggesting that we have a good fit.

The luminosity distance from the observational data is seemingly always lower than our data. This phenomena is known as the **Hubble tension** which is a widely known problem in today's standard model of cosmology [7]. Direct data, such as supernova data, seemingly always prefers lower values for luminosity distance, and thus, higher values for h that can be seen in FIG. 6. Indirect data, such as the CMB, however prefer higher values for d_L and thus lower values h with much smaller errorbars. This is an ongoing issue which suggests that the ΛCDM model is not a complete model and must be modified. The posterior PDF of the Hubble parameter today H_0 shows that the Gaussian fit is centered at roughly 70.1 km/s/Mpc. As mentioned, this is a large discrepancy from $H_0 = 67$ km/s/Mpc which we got from the fiducial cosmology but still considered a common result from direct data.

Next we consider the scatterplot in the $\Omega_{\Lambda}\Omega_{\mathrm{M}}$-plane shown in FIG. 7. The scatter-plot helps us visualize the degeneracy between the density parameters, i.e. that many different combinations of Ω_{M} and Ω_{Λ} can yield similar observational results. This leads to rather large

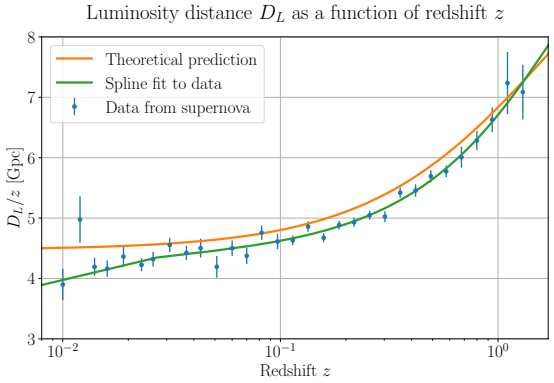

FIG. 5. Luminosity distance over redshift z, plotted against redshift z for both; our numerical data, and observational data from Betoule et. al. [3] with error-bars.

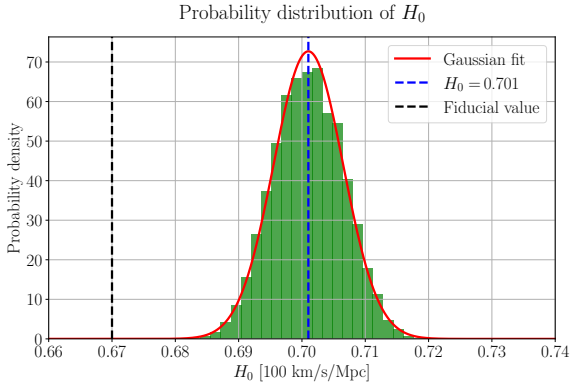

FIG. 6. Posterior PDF of the Hubble parameter H_0 compared to the fiducial value $H_0 = 67\,\mathrm{km/s/Mpc}$.

degenerate regions in the parameter space. In this figure we can see that the flat universe constraint significantly reduces this degeneracy by lowering the allowed parameters by multiple orders of magnitude. The figure clearly shows that $\Omega_{\Lambda 0} = 0$ is completely excluded given the observational data as this would be far outside the 2σ constraint. The best-fit value for $\Omega_{\mathrm{K}0} = 0.067$ tells us that the universe is seemingly quite flat, but that there is indeed some curvature. To test out whether this might just be an insensitivity to the $\Omega_{\mathrm{K}0}$ parameter the code was run again with a large initial value $\Omega_{\mathrm{K}0}$. The result did not seem to change whatsoever and thus this implies that our model is insensitive to the curvature of the universe.

1.5. Summary & Conclusion

To summarize this section, we numerically solved the ODEs for η and t past the radiation domination. We then computed $H(x)$ which gave us access to all the other relevant cosmological parameters. Further we checked that the numerical data corresponds to analytical approxima-

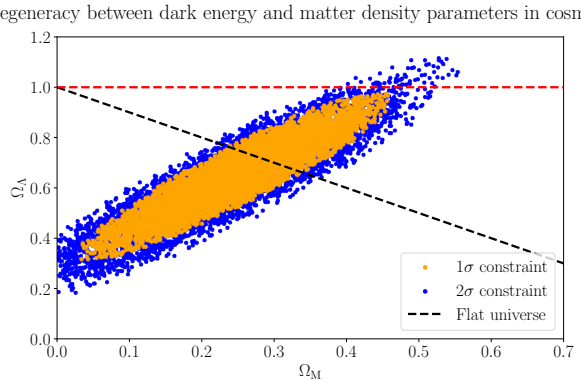

FIG. 7. Supernova data with 1σ and 2σ constraints from MCMC fits.

tions in the different regimes. Next we introduced all the most relevant data in a graphed form in FIG 4-6 such that important events and values were easily visualized. The most relevant values for the most important events in our background cosmology were summarized in TABLE I. Finally, an MCMC fit with observational data from supernova events and the numerical data in the $\Omega_\Lambda\Omega_\mathrm{M}$-plane was made to consider some important aspects of our model, in particular that we cannot consider a model without dark energy.

In conclusion, the data all seems to correspond quite well with observational data and previous calculations from more sophisticated methods.

2. MILESTONE II

Next we look at the recombination history of the universe. This is when baryons, mainly protons and electrons, went from being ionized to forming neutral atoms once the energy of the photons dropped below 13.6 eV. As a result, photons during this time decoupled from the thermal equilibrium of the universe and are what we now detect as the CMB photons. As this event is tightly related to the free mean path of photons, the goal of this section is to compute the optical depth τ, the visibility function $\tilde{g}$ and their derivatives. In this section we only consider the formation of hydrogen and neglect the existence of any heavier atoms.

To accomplish this we start by calculating the free electron fraction X_e which we will first compute from the **Saha equation** in early times till $X_e < 0.99$ and then switch over to the so-called **Peebles' equation** from thereon, both to be introduced later. The reason we don't use Peebles' equation from the start is due to it being extremely sensitive to high temperatures and thus the solution at early times is very unstable.

2.1. Theory

As eluded to in the intro we will consider the **optical depth** $\tau(x)$ which is defined by the relation:

$$I(r) = I_0 e^{-\tau(r)}, \tag{12}$$

where I_0 is the intensity of a source which emits radiation and $I(r)$ is the intensity that an observer at a distance r would detect. Here we can clearly see that if $\tau = 0$ then $I(r) = I_0$ and thus the medium the radiation travels through does not affect the intensity. If $\tau \gg 1$ then we say that the medium is **optically thick**, if $\tau \ll 1$ we say that the medium is **optically thin**, and $\tau \sim 1$ is the transition between the two.

In cosmology the main effect contributing to the optical depth is Thompson scattering of photons with free electrons. The optical depth can be related to the Thompson scattering cross section via:

$$\tau(\eta) = \int_{\eta}^{\eta_0} d\eta' \, n_e \sigma_T a, \tag{13}$$
$$\sigma_T = \frac{8\pi}{3} \frac{\alpha^2 \hbar^2}{m_e^2 c^2}$$

where n_e is the number density of free electrons. Note that since $\sigma_T \propto m^{-2}$ we have neglected the scattering cross section of Thompson scattering with protons due to their relatively large mass. (13) can be rewritten into differential form:

$$\frac{d\tau}{dx} = -\frac{c n_e \sigma_T}{H}, \tag{14}$$

which is the ODE that we will solve. Since optical depth is 0 today we have the initial condition $\tau(0) = 0$. On the right hand side of (14) the only missing factor is n_e. Instead of computing n_e directly we will consider the fractional electron density:

$$X_e \equiv n_e / n_H \approx \frac{n_e m_H}{\rho_b} = \frac{n_e m_H a^3}{\Omega_{\mathrm{B0}} \rho_{c0}},$$

where the approximation is due to us not considering any heavier elements than hydrogen. To do this we consider the Saha equation states:

$$\frac{n_e n_p}{n_e^0 n_p^0} = \frac{n_H n_\gamma}{n_H^0 n_\gamma^0},$$

where n_p, n_γ and n_H are the number densities for free protons, photons and Hydrogen atoms respectively and the superscript 0 represents that the given number density is in thermal equilibrium. This is an analytical approximation for when the interaction rate is very high compared to the change in electron density. Since in the early universe consists purely of free electrons due to the high temperatures of the primordial plasma, this then suggests that the Saha equation is only valid when $X_e \approx 1$. Given our definition of X_e and the approximations we can rewrite the Saha equation to the convenient form:

$$\frac{X_e^2}{1 - X_e} = \frac{1}{n_b} \left(\frac{k_b m_e T_b}{2\pi \hbar^2} \right)^{3/2} e^{-\epsilon_0 / k_b T_b}, \tag{15}$$

where T_b is the baryon temperature of the universe and $\epsilon_0 = 13.6\,\mathrm{eV}$ is the ionization energy of hydrogen. In reality there should also be a T_γ in this equation representing the temperature of photons at a given time, but due to their tight coupling at early times, in practice it is an excellent approximation to set $T_\gamma = T_b = T_{\mathrm{CMB0}}/a$ [1]. The rewritten Saha equation is now simply a 2nd order polynomial in X_e which is easily solved analytically:

$$X_e = \frac{C}{2} \left[\sqrt{1 + \frac{4}{C}} - 1 \right], \tag{16}$$
$$C \equiv \frac{1}{n_b} \left(\frac{k_b m_e T_b}{2\pi \hbar^2} \right)^{3/2} e^{-\epsilon_0 / k_b T_b}, \tag{17}$$

where we have omitted the negative solution due to the electron fraction being manifestly positive. We also note that in the limit $4/C \ll 1$ then $X_e = 1$ which will be used in numerical calculations later.

Since the Saha equation is only valid for $X_e \approx 1$ then, as noted earlier, we consider Peebles' equation outside this realm. The derivation for Peebles' equation is beyond the scope of this paper, but a simplified derivation can in [**?**] and is given by:

$$\frac{dX_e}{dx} = \frac{C_r(T_b)}{H} \left[\beta(T_b)(1 - X_e) - n_H X_e^2 \alpha^{(2)}(T_b) \right], \tag{18}$$

where

$$C_r(T_b) = \frac{\Lambda_{2s\to 1s} + \Lambda_\alpha}{\Lambda_{2s\to 1s} + \Lambda_\alpha + \beta^{(2)}(T_b)},$$
$$\Lambda_{2s\to 1s} = 8.227\,\mathrm{s}^{-1},$$
$$\Lambda_\alpha = H \frac{(3\epsilon_0)^3}{(8\pi)^2 c^3 \hbar^3 n_{1s}},$$
$$n_{1s} = (1 - X_e) n_H,$$
$$n_H = n_b, \text{ (no helium)}$$
$$n_b = \frac{3 H_0^2 \Omega_{b0}}{8\pi G m_H a^3},$$
$$\beta^{(2)}(T_b) = \beta(T_b) e^{\frac{3\epsilon_0}{4 k_b T_b}},$$
$$\beta(T_b) = \alpha^{(2)}(T_b) \left(\frac{m_e k_b T_b}{2\pi \hbar^2} \right)^{3/2} e^{-\frac{\epsilon_0}{k_b T_b}},$$
$$\alpha^{(2)}(T_b) = \frac{8}{\sqrt{3\pi}} c \sigma_T \sqrt{\frac{\epsilon_0}{k_b T_b}} \phi_2(T_b),$$
$$\phi_2(T_b) = 0.448 \ln \left(\frac{\epsilon_0}{k_b T_b} \right).$$

This ODE will then be solved numerically to find $X_e(x)$ with the initial condition given from the last X_e value

from the Saha solution. This then gives us $n_e(x)$ from the definition of X_e which will then be used to solve (14) for $\tau(x)$.

Further we consider the visibility function:

$$\tilde{g}(x) \equiv \frac{d}{dx} e^{-\tau(x)} = -e^{-\tau(x)} \tau'(x), \tag{19}$$

which turns out to be a probability density function. Since this is a probability density then it must satisfy:

$$\int_{-\infty}^{0} dx\, \tilde{g}(x) = 1.$$

The visibility function can be thought of as the probability that a photon scattering between time x and $x + dx$ is the last time it ever scatters before it moves freely. From this we can then consider the time of **last scattering** to occur when the visibility function peaks. Once the solution to $\tau(x)$ and its derivative has been established, getting the visibility function is a trivial task.

Finally we have the sound horizon $s(x)$ which is given by:

$$s(x) \equiv \int_0^a dt\, \frac{c_s}{a}, \tag{20}$$

where $c_s = c\sqrt{\frac{R}{3(1+R)}}$ is the sound-speed of the coupled photon-baryon plasma and

$$R = \frac{4\Omega_{\gamma 0}}{3a\Omega_{\mathrm{B}0}}. \tag{21}$$

To interpret the sound horizon we consider an overdense region of the primordial plasma. This region will cause gravitational wells which will further cause a surplus of interactions between photons and baryons. These interactions cause an outwards pressure until the interactions begin to slow down again. The gravitational wells formed by dark matter (as they do not feel this outward pressure) then get deeper, causing the same process to occur again. As such we will have oscillations of baryons and photons, which are comparable to propagating sound waves. The distance in which these sound waves may have travelled before recombination is what we define as the sound horizon. The reason why this quantity is particularly important is that once recombination occurs, the outward pressure will vanish. As such we expect to see overdensities begin to form on these rings after recombination.

We can rewrite (20) into a differential form as such:

$$\frac{ds}{dx} = \frac{c_s}{\mathcal{H}}, \tag{22}$$

Notice that in radiation domination we have that $R \to \infty$, implying that the sound speed $c_s = c/\sqrt{3}$. As such we obtain the initial condition:

$$s(x_{\mathrm{ini}}) = \frac{c_s(x_{\mathrm{ini}})}{\mathcal{H}(x_{\mathrm{ini}})} = \frac{c}{\sqrt{3}} \mathcal{H}^{-1}(x_{\mathrm{ini}}).$$

2.2. Implementation details

2.2.1. Solving the Saha and Peebles' equation

We began by implementing a `for`-loop for the Saha equation which at each iteration checks whether we are still in the Saha regime. Note that we have to be careful about round-off errors when solving the Saha equation. When $\epsilon_0/k_b T_b \to 0$ in the exponential in (17), the rest of the expression will begin to explode. Thus in (16) we would be subtracting two very large numbers, which should at the end simplify to just 1, leading to potential round-off errors. To avoid this we instead performed an `if`-test to check whether $4/C$ is less than some small threshold. Once this is the case then we simply set X_e to 1 justified by considering the first order expansion of the square root in (16), which will just yield $X_e = 1$. Since the Saha equation is only valid for $X_e \approx 1$, we decide to switch over to the more accurate Peebles' equation $X_e < 0.99$. For reference we continued on with the Saha equation past its validity to compare the results.

Peebles' equation was then solved numerically via the same ODE solver used in the previous milestone with the initial condition supplied by the last point before we exited the Saha regime. Some care was taken to ensure no overflow due to the exponential in the $\beta^{(2)}$ equation under (18). To do this we simply created another `if`-test to check when the term in the exponential exceeded 150 and set $\beta^{(2)} = 0$ as the exponential from β will dominate over it. We then had the results for X_e which we used to compute n_e for both cases. The results for both the Saha only and the Saha-Peebles computations were splined and printed to a data file.

2.2.2. Solving for the optical depth and visibility functions

Next we solved the ODE for both the optical depth $\tau(x)$ in eq. 14 and the sound-horizon $s(x)$ with the before mentioned initial conditions. Note that the prior ODE, if computed it in the usual way, one would need to subtract an initial condition off the solution for $\tau(x = 0)$ which would lead to round-off errors close to $x = 0$ due to the finite precision of floating point numbers. This would then lead to noise in the solution. Thus the ODE was then instead solved by going backwards in time to avoid this problem. After, $\tau'(x)$ was also computed since the spliner we are working with seemingly does not work well past 1st derivatives since we also want to consider $\tau''(x)$. With both $\tau(x)$ and $\tau'(x)$ we could easily calculate the visibility function $\tilde{g}(x)$ with (19) and its first derivative. These were then all splined along with using the `deriv_x` function in the spliner s.t. we have access to the 2nd derivatives. All the data was again printed to the aforementioned data file.

With the various splines we then calculated the time at recombination and last scattering. Our definition for when recombination happens is when X_e drops below

0.1 and the definition for when last scattering occured is when $\tilde{g}$ peaks. This was done by iterating through the data in `C++` until these conditions were met.

As previously, the data was imported to Python and various plots together with a table of the various events were made.

2.3. Results

2.3.1. Recombination Events

We first consider the quantities x, z, y and r_s at both recombination and when last scattering occurred. The results are summarized in TABLE II. The times for recombination and last scattering both are in agreement previously found values [2].

TABLE II. Recombination Events

Event	x	z	t [kyr]	r_s [Mpc]
Recombination	-6.9855	1079.8	377.96	145.278
Last scattering	-6.9853	1079.7	378.04	145.292

2.3.2. Electron Fraction X_e

The results for the electron fraction X_e are given in FIG. 8. Here we see that the moment the electron fraction deviates even a small amount from $X_e = 1$ then the Saha equation plummets, suggesting that recombination would happen at some time $x \sim -7.14$ instead of the value given in TABLE II with Peebles' more accurate equation. In this figure, freeze out refers to the present day abundance of free electron which we find to be $X_e(0) \approx 2.03 \cdot 10^{-4}$.

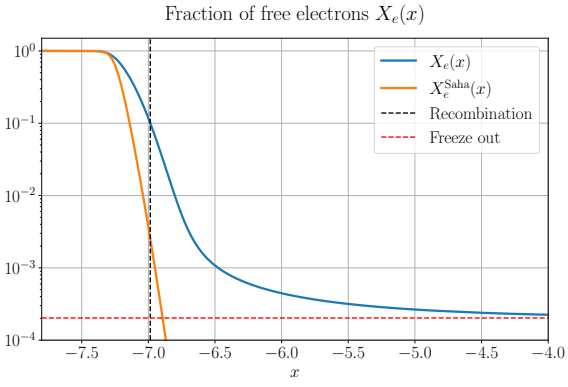

FIG. 8. Time evolution of the free electron fraction $X_e(x)$.

2.3.3. Evolution of Optical Depth and Visibility function

Further we consider the time evolution of the optical depth parameter, the visibility function and their derivatives given in FIG. 9 and 10 respectively. The negative of the first derivative of τ is plotted s.t. we can read off all of them in a single log-plot. For a similar reason the derivatives of $\tilde{g}$ are normalized such that their peak is at $\max \tilde{g}$. The surface of last scattering with the $\tilde{g}$ peak definition is shown for reference.

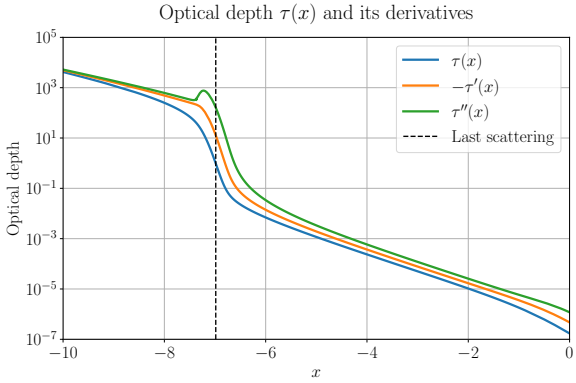

FIG. 9. Time evolution of the optical depth $\tau(x)$ and its derivatives.

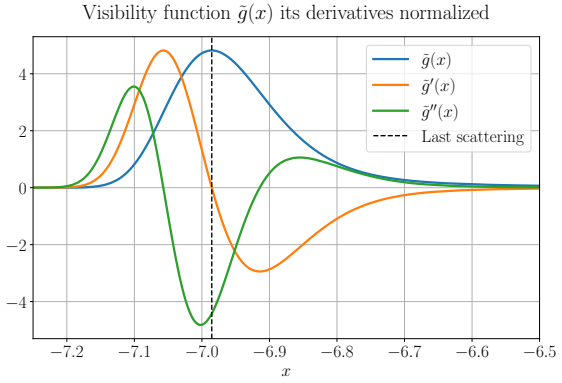

FIG. 10. Time evolution of visibility function $\tilde{g}$ and its derivatives all normalized s.t. $\max|\tilde{g}| = \max|\tilde{g}'| = \max|\tilde{g}''|$ So that it all fits in the same plot. These scale factors are roughly 10 and 200 for $\tilde{g}'$ and $\tilde{g}''$ respectively.

Before this dashed line signaling the last scattering event, the primordial plasma is optically thick. Thus the mean free path of photons is too short and will continue scattering. However, the optical depth at this time still endures a stable decay almost solely due to the expansion rate of the universe as this causes the number density n_e to decrease which can be seen in (13). As mentioned previously, the visibility function is the probability density that a given photon had its last scattering at time x. Thus we can see that when the optical depth is very

high, the likelihood of a particular photon at that time scattering for the last time is very small.

$\tau(x)$ then dips down violently as the number of free electrons in the universe rapidly decays. At the same time we then see that this is when the visibility function begins to rapidly increase. This clearly shows that the formation of neutral Hydrogen happens much faster than the expansion of the universe, hence having the largest effect in this epoch. This in turn means that the mean free paths of photons increase beyond their immediate vicinity and thus, photons are effectively free to travel without interacting with matter. This is when the last scattering event occurs and the photons released here are the ones that we detect today in the CMB spectra.

Once the electron fraction begins to flatten out again, the optical depth becomes a straight line on the log-plot, once again caused by the expansion of the universe. The visibility function also begins to flatten out at this point, albeit at a slower rate than the initial increase before last scattering.

2.4. Summary & Conclusion

We first solved the Saha equation due to Peebles' equation being stiff when the temperature of the universe was very high. We then switched over to use Peebles' equation once the fractional electron number density dropped sufficiently low. We then proposed times for when recombination and last scattering occurred within our model. At last we had a discussion of the optical depth and the visibility function along with their physical relevance.

We can readily note from FIG. 10 that recombination and last scattering did not happen instantaneously, as $\tilde{g}(x)$ would take the form of a Dirac-delta function, but instead over a relatively short period of time. Due to the short time frame, the number of free electrons in the universe rapidly decreased over several orders of magnitude. The values in TABLE II show us that recombination generally happens first, with the last scattering following shortly after.

As expected from the assumptions made in the derivation of the Saha equation, we see that it quickly becomes a terrible approximation outside of its regime. The manifestly seen correlation between the change in fraction of free electrons, optical depth and the visibility function is also clearly seen, but is of no surprise from their various relations.

3. MILESTONE III

The topic of this section is to see how small quantum fluctuations from the inflationary period caused small perturbations to the baryon, photon and dark matter fluid in the early which then grew into large structures formations we see today. Since we have determined various quantities of the background cosmology in the previous sections, all we need to do it to perturb the background. To do this we write the perturbed flat FRLW metric in the Newtonian gauge.

3.1. Theory

3.1.1. Metric perturbations

As mentioned in the intro we consider perturbations to the flat FLRW metric:

$$g_{\mu\nu} = g^0_{\mu\nu} + h_{\mu\nu}, \qquad |h_{\mu\nu}| \ll 1,$$

where $g^0_{\mu\nu}$ is the pure FLRW metric and $h_{\mu\nu}$ is a small perturbation. By $|h_{\mu\nu}| \ll 1$ we mean that there exists some coordinate system where the components of $h_{\mu\nu}$ satisfy this. The Newtonian gauge in Cartesian coordinates is defined by:

$$h_{00} = -2\Psi, \quad h_{0i} = 0, \quad h_{ij} = 2a^2\delta_{ij}\Phi,$$

where $\Psi = \Psi(t, \mathbf{x})$ and $\Phi = \Phi(t, \mathbf{x})$ are scalar perturbations of the flat FRLW metric which happen to be the Newtonian potential and the Newtonian curvature respectively, which can be seen by considering the Newtonian limit. Note that this implies that $\Psi \ll 1$ and $\Phi \ll 1$. As such the line element in the Newtonian gauge takes the form:

$$ds^2 = -(1 + 2\Psi)dt^2 + a^2(t)(1 + 2\Phi)d\mathbf{x}^2.$$

3.1.2. Photon temperature fluctuations

Since we are interested in solving perturbations to the Boltzmann equations for the various particle types we first consider the Boltzmann equation for photons:

$$\frac{df}{dt} = C[f],$$

where $f = f(\mathbf{x}, \mathbf{p}, t)$ is the Bose-Einstein distribution due to photons being relativistic integer spin particles and $C[f]$ is the collision term due to Thompson scattering. Expanding the total derivative on the left via the chain rule yields:

$$\frac{df}{dt} = \frac{\partial f}{\partial t} + \frac{\partial f}{\partial \mathbf{x}}\frac{d\mathbf{x}}{dt} + \frac{\partial f}{\partial |\mathbf{p}|}\frac{d|\mathbf{p}|}{dt} + \frac{\partial f}{\partial \hat{\mathbf{p}}}\frac{d\hat{\mathbf{p}}}{dt}, \tag{23}$$

where $\hat{\mathbf{p}} = \mathbf{p}/|\mathbf{p}|$ is the direction of the photon propagation. Using the geodesic equation and the metric whilst only keeping first order terms, one can show that (23) can be rewritten to a more convenient form:

$$\frac{df}{dt} = \frac{\partial f}{\partial t} + \frac{p}{E}\frac{\hat{\mathbf{p}}}{a}\frac{\partial f}{\partial \mathbf{x}} - |\mathbf{p}|\frac{\partial f}{\partial |\mathbf{p}|}\left[H + \frac{d\Phi}{dt} + \frac{E}{a}\frac{\hat{\mathbf{p}}}{|\mathbf{p}|}\frac{\partial \Psi}{\partial \mathbf{x}}.\right]$$

Since we know the CMB is roughly $T^0 = 2.7255\,\mathrm{K}$ with small fluctuations around this average, we then define the perturbation about this equilibrium:

$$T(\mathbf{x}, \hat{\mathbf{p}}, t) = T^0[1 + \Theta(\mathbf{x}, \hat{\mathbf{p}}, t)].$$

One can show that all terms dependent on the magnitude of the momenta stemming from the Boltzmann equation for photons, can be rewritten in terms of Ψ and Φ to first order, or are of second order or higher and thus discarded. As such the collision term for Thompson scattering in the Boltzmann equation then takes the form:

$$C[f(\mathbf{p})] = -p\frac{\partial f^0}{\partial p} n_e \sigma_T [\Theta_0 - \Theta(\hat{\mathbf{p}}) + \hat{\mathbf{p}} \cdot \mathbf{v}_b], \tag{24}$$

where $\mathbf{v}_b$ is the bulk velocity of baryons. A more in-depth derivation can be found in [**?**]. As mentioned in the prior section, we can ignore the contributions from protons as $m_p \gg m_e$ since the Thompson cross section $\sigma_T \propto m^{-2}$. Thus in practice it really only specifies the bulk velocity of electrons before recombination. The other side of the Boltzmann equation for photons to first order is:

$$\frac{df}{dt} = -p\frac{\partial f^0}{\partial p}\left[\frac{\partial \Theta}{\partial t} + \frac{\hat{\mathbf{p}}}{a}\frac{\partial \Theta}{\partial \mathbf{x}} + \frac{d\Phi}{dt} + \frac{\hat{\mathbf{p}}}{a}\frac{\partial \Psi}{\partial \mathbf{x}}\right]. \tag{25}$$

Equating (24) and (25) yields the Boltzmann equation for radiation to first order:

$$\frac{\partial \Theta}{\partial t} + \frac{\hat{\mathbf{p}}}{a}\frac{\partial \Theta}{\partial \mathbf{x}} + \frac{d\Phi}{dt} + \frac{\hat{\mathbf{p}}}{a}\frac{\partial \Psi}{\partial \mathbf{x}} = n_e \sigma_T [\Theta_0 - \Theta(\hat{\mathbf{p}}) + \hat{\mathbf{p}} \cdot \mathbf{v}_b]. \tag{26}$$

3.1.3. Matter density and velocity fluctuations

Next we consider the Boltzmann equation for CDM. As mentioned in previous sections we consider CDM to be WIMPs, meaning their collision term is simply null. As mentioned earlier, CDM are non-relativistic particles, and thus their distribution function can be modelled as a Maxwell-Boltzmann distribution. Considering them to act as a perfect liquid and following a similar procedure one arrives at the cosmological generalization of the continuity equation and Euler equation respectively:

$$0 = \frac{\partial n}{\partial t} + \frac{1}{a}\frac{\partial (n\mathbf{v})}{\partial \mathbf{x}} + 3n\left[H + \frac{\partial \Phi}{\partial t}\right], \tag{27}$$

$$0 = \frac{\partial \mathbf{v}}{\partial t} + H\mathbf{v} + \frac{1}{a}\frac{\partial \Psi}{\partial \mathbf{x}}, \tag{28}$$

where we have suppressed the label CDM on the number density $n \equiv n_{\mathrm{CDM}}$ and the bulk velocity $\mathbf{v} \equiv \mathbf{v}_{\mathrm{CDM}}$ for readability. Further considering perturbations about the mean number density n^0:

$$n(\mathbf{x}, t) = n^0[1 + \delta(\mathbf{x}, t)],$$

the first order contribution to (**??**) is then:

$$\frac{\partial \delta}{\partial t} + \frac{1}{a}\frac{\partial \mathbf{v}}{\partial \mathbf{x}} + 3\frac{\partial \Phi}{\partial t} = 0. \tag{29}$$

Baryons are also considered to behave and a non-relativistic fluid, meaning they satisfy Maxwell-Boltzmann distributions. The main difference between baryons and CDM is that they can interact amongst themselves and photons, the latter being via Thompson scattering. However as mentioned previously, Thompson scattering via protons can be neglected due to the cross section being inversely proportional to the square of the mass of the scattered particle. The perturbations to the cosmological continuity equation takes the same form as (29), i.e.:

$$\frac{\partial \delta_{\mathrm{B}}}{\partial t} + \frac{1}{a}\frac{\partial \mathbf{v}_{\mathrm{B}}}{\partial \mathbf{x}} + 3\frac{\partial \Phi}{\partial t} = 0. \tag{30}$$

However the corresponding Euler equation takes a different form due to interactions:

$$\frac{\partial \mathbf{v}_{\mathrm{B}}}{\partial t} + H\mathbf{v}_{\mathrm{B}} + \frac{1}{a}\frac{\partial \Psi}{\partial \mathbf{x}} = -n_e \sigma_T R(\mathbf{v}_\gamma - \mathbf{v}_{\mathrm{B}}), \tag{31}$$

where R is defined in (21) and the parenthesis on the right hand side corresponds to the momentum transfer in the scattering process.

3.1.4. Fourier transform and multipole expansions

As of now all the relevant equation are all partial differential equations (PDEs) which remain tough to solve. Thus we wish to express these in terms of ODEs instead as this is something we know how to solve. We first consider the temperature perturbations Θ. Since we are in general interested in the perturbations on various different scales in a mostly spherically symmetric universe we consider rewriting our functions in terms of multipole expansions. These are a series written in terms of Legendre polynomials $P_l(\lambda \equiv \cos\theta)$:

$$\Theta(t, k, \lambda) = \sum_{l=0}^{\infty} \frac{2l+1}{i^l}\Theta_l(t, k)P_l(\lambda).$$

The Legendre polynomials are orthonormal and form a complete basis. As such we can invert this equation in the same way as one would for Fourier coefficients to attain the Legendre multipoles:

$$\Theta_l(t, k) = \frac{i^l}{2}\int_{-1}^{1} d\lambda\, \Theta(t, k, \lambda)P_l(\lambda).$$

The most relevant moments are: the monopole $\Theta_0 = \frac{1}{4}\delta_\gamma$, the dipole $\Theta_1 = -\frac{1}{3}v_\gamma$ and the quadrupole Θ_2. One can then recursively find all the Legendre polynomials by using Bonnet's recursion formula:

$$\lambda P_l = \frac{l+1}{2l+1}P_{l+1} + \frac{l}{2l+1}P_{l-1}.$$

Then, bringing (26) into Fourier space, switching to conformal time, using the above mentioned tricks together

with the orthonormality of the Legendre polynomials, rewriting everything in terms of x, and reintroducing SI-units one find that the time dependence of the multipoles are given by:

$$\begin{aligned}
\Theta_0' &= -\frac{ck}{\mathcal{H}}\Theta_1 - \Phi', \\
\Theta_1' &= \frac{ck}{3\mathcal{H}}\Theta_0 - \frac{2ck}{3\mathcal{H}}\Theta_2 + \frac{ck}{3\mathcal{H}}\Psi + \tau'\left[\Theta_1 + \frac{v_{\mathrm{B}}}{3}\right], \\
\Theta_l' &= \frac{lck}{(2l+1)\mathcal{H}}\Theta_{l-1} - \frac{(l+1)ck}{(2l+1)\mathcal{H}}\Theta_{l+1}, \\
&\quad + \tau'\left[\Theta_l - \frac{\Theta_l}{10}\delta_{l,2},\right],
\end{aligned}$$

where the primes, as before, now represent derivatives w.r.t. $x = \ln(a)$, k is the corresponding Fourier coefficient and v is defined via the relation $\mathbf{v} = i\hat{\mathbf{k}}v$.

Next we consider the scalar potentials Φ and Ψ which can be found from the EFE. After some work one arrives at the following equations:

$$\begin{aligned}
\Phi' &= \Psi - \frac{1}{3}\left(\frac{ck}{\mathcal{H}}\right)^2\Phi + \frac{1}{2}\left[\delta\Omega_{\mathrm{CDM}} + \delta_{\mathrm{B}}\Omega_{\mathrm{B}} + \delta_\gamma\Omega_\gamma\right], \\
\Psi &= -\Phi - 12\left(\frac{\mathcal{H}}{ck}\right)^2\Omega_\gamma\Theta_2.
\end{aligned}$$

An in-depth derivation for this result can be seen in [**?**].

Further, to simplify the problem of solving number density perturbations δ and bulk velocity v for baryons and CDM we begin by expressing them in terms of conformal time and further translate them over to Fourier space to arrive at:

$$\begin{aligned}
\dot{\delta} &= -3\dot{\Phi} + kv, \\
\dot{v} &= -k\Psi - \mathcal{H}v, \\
\dot{\delta}_{\mathrm{B}} &= -3\dot{\Phi} + kv_{\mathrm{B}}, \\
\dot{v}_b &= -k\Psi + \dot{\tau}R(v_{\mathrm{B}} - v_\gamma) - \mathcal{H}v_{\mathrm{B}}.
\end{aligned}$$

As before we switch over to our time variable x and use some of the relations between the multipoles. The results are summarized in equations (32, 33, 34) where $l_{\max}$ refers to the highest order multipole which we compute.

Photon temperature multipoles

$$\Theta_0' = -\frac{ck}{\mathcal{H}}\Theta_1 - \Phi', \tag{32a}$$

$$\Theta_1' = \frac{ck}{3\mathcal{H}}\Theta_0 - \frac{2ck}{3\mathcal{H}}\Theta_2 + \frac{ck}{3\mathcal{H}}\Psi + \tau'\left[\Theta_1 + \frac{1}{3}v_{\mathrm{B}}\right], \tag{32b}$$

$$\Theta_2' = \frac{2ck}{5\mathcal{H}}\Theta_1 - \frac{3ck}{5\mathcal{H}}\Theta_3 + \frac{9}{10}\tau'\Theta_2, \tag{32c}$$

$$\Theta_l' = \frac{lck}{(2l+1)\mathcal{H}}\Theta_{l-1} - \frac{(l+1)ck}{(2l+1)\mathcal{H}}\Theta_{l+1} + \tau'\Theta_l, \tag{32d}$$

Above is valid for $2 < l < l_{\max}$,

$$\Theta_{l_{\max}}' = \frac{ck}{\mathcal{H}}\Theta_{l-1} - c\frac{l+1}{\mathcal{H}\eta}\Theta_l + \tau'\Theta_l. \tag{32e}$$

CDM and baryons

$$\delta' = \frac{ck}{\mathcal{H}}v - 3\Phi', \tag{33a}$$

$$v' = -v - \frac{ck}{\mathcal{H}}\Psi, \tag{33b}$$

$$\delta_{\mathrm{B}}' = \frac{ck}{\mathcal{H}}v_{\mathrm{B}} - 3\Phi', \tag{33c}$$

$$v_{\mathrm{B}}' = -v_{\mathrm{B}} - \frac{ck}{\mathcal{H}}\Psi + \tau'\,R(3\Theta_1 + v_{\mathrm{B}}). \tag{33d}$$

Metric perturbations

$$\Phi' = \Psi - \frac{c^2k^2}{3\mathcal{H}^2}\Phi + \frac{1}{2}[\delta\Omega_{\mathrm{CDM}} + \delta_{\mathrm{B}}\Omega_{\mathrm{B}} + 4\Omega_\gamma\Theta_0], \tag{34a}$$

$$\Psi = -\Phi - \frac{12\mathcal{H}^2}{c^2k^2}\Omega_\gamma\Theta_2. \tag{34b}$$

We have now removed all spatial dependency and are instead expressed in terms of the Fourier mode k. These modes now, instead of representing the spatial distribution, represent a unique spatial scale. Since Fourier modes in general are related to frequency, which is inversely proportional to wavelength, then $k \sim 1/\lambda$ where λ is the relevant length scale. As such this is a very efficient way to look at what exactly happens at different cosmological scales. One can also relate these various scales to the Horizon to see what scales are causally connected and disconnected by considering the quantity $k\eta$. If $k\eta \gg 1$ then we are working with scales much smaller than the horizon, if $k\eta \ll 1$ these scales are much larger than the horizon and represent acausal distances. Finally $k\eta \simeq 1$ is the scale at which the mode relates quantities which are the same magnitude as the horizon.

3.1.5. Tight coupling

One particular problem behind the set of differential equations in the very early universe $\tau' \gg 1$. Before recombination when both radiation, and baryons where tightly coupled due to the primordial plasma being optically thick. $\tau \gg 1$ implies that baryons in the early universe only interacts with its close neighbourhood. This is what we consider the **tight coupling regime**. This in turn causes the set of differential equations to be numerically unstable. To remedy this we instead attempt to consider a numerically stable approximation for $\Theta_1 + \frac{1}{3}v_\mathrm{B}$ in this regime. Adding together $3\times$(32b) and (33d) yields:

$$[3\Theta_1 + v_\mathrm{B}]' = \frac{ck}{\mathcal{H}}(\Theta_0 - 2\Theta_2) + \tau'(1+R)[3\Theta_1 + v_\mathrm{B}] - v_\mathrm{B}. \tag{35}$$

Taking the next derivative of this, using $R' = -R$ and (33d) again to get rid of $-v_\mathrm{B}'$ we arrive at:

$$\begin{aligned}[3\Theta_1 + v_\mathrm{B}]'' = &-\frac{ck}{\mathcal{H}}\frac{\mathcal{H}'}{\mathcal{H}}(\Theta_0 - 2\Theta_2) + \frac{ck}{\mathcal{H}}(\Theta_0 - 2\Theta_2)' \\ &+ (\tau''(1+R) - R\tau')[3\Theta_1 + v_\mathrm{B}] \\ &+ (\tau'(1+R) - 1)[3\Theta_1 + v_\mathrm{B}]' + 3\Theta_1'.\end{aligned}$$

Substituting in the equation for Θ_1' and approximating that $(3\Theta_1 + v_\mathrm{B}) \propto \tau'^{-1} \propto \eta$ which holds during radiation domination. This implies that:

$$[3\Theta_1 + v_\mathrm{B}]'' \approx -\frac{\mathcal{H}'}{\mathcal{H}}[3\Theta_1 + v_\mathrm{B}]'.$$

Then solving for $q \equiv [3\Theta_1 + v_\mathrm{B}]'$ we arrive at:

$$\begin{aligned}q = &-\frac{1}{\tau'(1+R) + \frac{\mathcal{H}'}{\mathcal{H}} - 1}\times \\ &\Bigg[(\tau''(1+R) + (1-R)\tau')[3\Theta_1 + v_b] \\ &+ \frac{ck}{\mathcal{H}}\left(\Psi + \Theta_0' - 2\Theta_2' + \left(1 - \frac{\mathcal{H}'}{\mathcal{H}}\right)(\Theta_0 - 2\Theta_2)\right)\Bigg].\end{aligned}$$

One can however show that $\Theta_2' \sim 3\Theta_2 \ll \Theta_0$ during this epoch, thus we can ignore this term. In fact we will ignore the explicit time evolution of all multipoles of higher order than the dipole in this regime. We will however implicitly evolve them as these higher order multipoles do depend on the evolution of Θ_0 and Θ_1. Further we can solve for $\tau'(1+R)[3\Theta_1 + v_\mathrm{B}]$ by using (35) and substitute this into the equation for v_B' to give us:

$$v_\mathrm{B}' = \frac{1}{1+R}\left[R\left(q + \frac{ck}{\mathcal{H}}(2\Theta_2 - \Theta_0 - \Psi)\right) - v_\mathrm{B} - \frac{ck}{\mathcal{H}}\Psi\right].$$

With this we arrive at a set of equations which we expect to hold before recombination, summarized in (36). Note however that the equations for $\Theta_0', \delta', v', \delta_\mathrm{B}'$ and Φ' remain the same in this regime as they are numerically stable. The equations for Θ_l with $l \geq 2$ come from the initial conditions, to be discussed later.

Tight coupling regime

$$\begin{aligned}&q\left[(1+R)\tau' + \frac{\mathcal{H}'}{\mathcal{H}} - 1\right] \\ &\quad = -\left[\tau''(1+R) + \tau'(1-R)\right](3\Theta_1 + v_\mathrm{B}) \\ &\quad -\frac{ck}{\mathcal{H}}\left[\Psi + \Theta_0' - \left(1 - \frac{\mathcal{H}'}{\mathcal{H}}\right)(2\Theta_2 - \Theta_0)\right] \quad (36a)\end{aligned}$$

$$\begin{aligned}v_\mathrm{B}[1+R] = &R\left(q + \frac{ck}{\mathcal{H}}(2\Theta_2 - \Theta_0 - \Psi)\right) \\ &- v_\mathrm{B} - \frac{ck}{\mathcal{H}}\Psi \quad (36b)\end{aligned}$$

$$\Theta_1' = -\frac{1}{3}(q - v_\mathrm{B}') \quad (36c)$$

$$\Theta_2 = -\frac{20ck}{45\mathcal{H}\tau'}\Theta_1 \quad (36d)$$

$$\Theta_l = -\frac{l}{2l+1}\frac{ck}{\mathcal{H}\tau'}\Theta_{l-1}, \quad l \geq 2 \quad (36e)$$

3.1.6. Inflation

To begin solving the various differential equations we of course need initial conditions. This is done by considering what conditions the universe satisfies once inflation ends.

In the CMB spectra we see today there is seemingly a correlation between the photon temperature fluctuations on acausal scales. Together with this we observationally have a universe which is flat to a very high degree of confidence. Thus would in turn cause a huge fine tuning problem in the early universe as the "flatness" of the universe would decrease over time. To explain these observational phenomena we consider a universe which expanded exponentially for a short time frame in the very early universe. This is what is known as inflation. This event would allow for an initially non-flat universe together with allowing for relatively large scales to be within the horizon at very early times to allow for interactions, causing correlations between them. Then moments later the universe exponentially expands causing the universe to appear flat on smaller scales (such as the observable universe today) and would drive correlations between what would today seem like acausal scales.

We assume that inflation is driven by a scalar quantum field ϕ which we call the inflaton field. By assuming that we can model the collection of inflaton as a perfect fluid along with assuming that the early universe was dominated by this inflaton field. With these assumptions the Friedmann equations yield that the inflaton must have an equation of state such that $p < -\rho/3$, i.e. the inflaton field must have a sufficiently negative pressure. By considering the Lagrangian for the inflaton field together

with its stress-energy tensor: [**?**]

$$T^{\mu}{}_{\nu} = g^{\mu\rho}\frac{\partial\phi}{\partial x^{\rho}}\frac{\partial\phi}{\partial x^{\nu}} - \delta^{\mu}_{\nu}\left[\frac{1}{2}g^{\rho\sigma}\frac{\partial\phi}{\partial x^{\rho}}\frac{\partial\phi}{\partial x^{\sigma}} + V(\phi)\right],$$

one can obtain the following relations for the energy density and pressure:

$$\rho_{\phi} = \frac{1}{2}\left(\frac{d\phi}{dt}\right)^2 + V(\phi),$$
$$p_{\phi} = \frac{1}{2}\left(\frac{d\phi}{dt}\right)^2 - V(\phi),$$

where $V(\phi)$ is the potential energy of the inflaton field. The restriction on the equation of state suggests that the inflaton field must have more potential energy than kinetic energy. In order to avoid a rapid phase transition of the inflaton field to not mess with potential observation we then consider a slow roll down the potential.

To account for the small fluctuations in the CMB spectra we assume that these are initially caused by tiny quantum fluctuations of the inflaton fields. To do this we write:

$$\phi(t, \mathbf{x}) = \phi^0(t) + \delta\phi(t, \mathbf{x}),$$

where ϕ^0 is the equilibrium of the field and $\delta\phi$ is a small perturbation, not to be confused with the perturbed number density for CDM. To proceed from here we consider a conserved quantity during throughout the inflationary epoch:

$$\xi = -\frac{ik^i\delta T^0_i H}{k^2(\rho + p)} - \Psi, \tag{37}$$

where k_i is the Fourier mode. At a time t_i before inflation we assume that the universe is perfectly FLRW, i.e. $\Phi = \Psi = 0$, one arrives at:

$$\xi(t_i) = -aH\frac{\delta\phi}{\dot{\phi}},$$

where we temporarily refer to $\dot{\phi} \equiv \frac{d\phi}{dt}$ instead of w.r.t. η. Using the conserved quantity again at t_f representing the end of equation where we now assume that radiation domination has begun then we have:

$$\xi(t_f) = -\frac{3}{2}\Psi.$$

Equating the two we then have an initial value for Ψ at the time where the mode k crosses the horizon:

$$\Psi = \frac{2}{3}\,\mathcal{H}\frac{\delta\phi}{\dot{\phi}}\bigg|_{\mathcal{H}=k}. \tag{38}$$

The FRLW perturbed Klein-Gordon equation for the inflaton can then be found to be:

$$\delta\ddot{\phi} + 2\mathcal{H}\delta\dot{\phi} + k^2\delta\phi = 0.$$

Quantizing ϕ and solving this damped harmonic oscillator equation then allows us to relate $\delta\phi$ to all the other quantities.

3.1.7. Initial conditions

We can now determine initial conditions to allow us to solve the full system. We have made a connection between the Newtonian scalar Φ and the perturbations in the inflaton field $\delta\phi$. As such, all that remains is to connect Φ to the rest of our parameters. To do this we make the assumptions that we have either adiabatic initial conditions, i.e. that the density fluctuations are present at the end of inflation, or that we have isocurvature perturbations, i.e. that fluctuations are generated from casual interactions of matter. For adiabatic perturbations, the number density of each species is the same everywhere:

$$\frac{n_i}{n_{\gamma}} = \frac{\bar{n}_i}{\bar{n}_{\gamma}},$$

where i represents the particle type. Since $\bar{\rho}_i(a) \propto a^{-3(1+\omega_i)}$ [8] we have that:

$$\rho_i(x, a) = \bar{\rho}_i(a + \delta a(x)) \simeq \bar{\rho}_i(a)(1 - 3a^{-1}(1 + \omega_i)\delta a).$$

As such we have that $\delta_i(x, a) = -3a^{-1}(1 + \omega_i)\delta a$ which then yields that, for any species i, j, the following relation holds:

$$\frac{\delta_i}{1 + \omega_i} = \frac{\delta_j}{1 + \omega_j}.$$

Using this on our various particle species we have that $4\Theta_0 = \delta_{\mathrm{B}} = \delta$. Further, connecting this to Φ and Ψ we have that at very early times:

$$k\eta \simeq \frac{ck}{\mathcal{H}} \ll 1 \leftrightarrow k \ll \mathcal{H},$$
$$\tau \gg 1 \quad |\tau'| \gg 1.$$

The first is necessary ensure that there exist causally disconnected regions in the early universe, the second is early established in the prior section. Noting that the metric perturbation evolve very slowly outside the horizon, we have $\Phi \approx \Psi \approx 0$. The Poisson equation then yields $2\Theta_0 \simeq -\Psi$. This is then used to connect all the various particle types to Ψ and hence Φ. Next we have the velocity equations. The equation for the CDM velocity can be rewritten:

$$(ve^x)' = -\frac{cke^x}{\mathcal{H}}\Psi.$$

Integrating this and throwing away a term Ce^{-x} [which I dont think I can justify by saying its a "decaying mode" as when $x \to -\infty$ this explodes. Would like to hear another reasoning for being able to discard this term.] we arrive at:

$$v = -\frac{ck}{2\mathcal{H}}\Psi.$$

Similar arguments work for baryons and Θ_1. The arguments for the general Θ_l is a little more involved, but an analytical approximation yields:

$$\Theta_l \simeq -\frac{l}{2l+1}\frac{ck}{\mathcal{H}\tau'}\Theta_{l-1}, \quad l > 2.$$

Here we can see that $\Theta_{l+1} \propto \tau'^{-l}$ for $l > 0$, as such this implies that $\Theta_l \gg \Theta_{l+1}$ which justifies the assumptions made in the tight coupling regime.

Now that everything is related to Φ and Ψ, all we need to do is to specify some normalization for these. Since the set of equations, even in the full regime, is linear we can freely choose the normalization of the system at this stage. As such one cannot make take any physical meaning from the numerical values of any of the quantities from here on and only their relative quantities until we insert this factor back later in the final section. Note that this includes removing any phase from the various Fourier transformed quantities, but we will in general only be working with the power spectrum which involves the absolute value squared.

For a mode outside the horizon in the radiation era we have that:

$$\xi \simeq \Phi - \frac{1}{2}\Psi,$$

where ξ was defined (37). The relation of the two potentials is given by: [**?**]

$$\Phi + \Psi \simeq 0,$$

if one ignores neutrinos. If we then set the normalization of $\xi = 1$ then we have $\Phi \simeq -\Psi \simeq \frac{2}{3}$. Rewriting everything in terms of Ψ we have the full set of initial conditions summarized in (39).

Initial conditions

$$\Psi = -\frac{2}{3} \tag{39a}$$
$$\Phi = -\Psi \tag{39b}$$
$$\delta = \delta_{\mathrm{B}} = -\frac{3}{2}\Psi \tag{39c}$$
$$v = v_{\mathrm{B}} = -\frac{ck}{2\mathcal{H}}\Psi \tag{39d}$$
$$\Theta_0 = -\frac{1}{2}\Psi \tag{39e}$$
$$\Theta_1 = \frac{ck}{6\mathcal{H}}\Psi \tag{39f}$$
$$\Theta_2 = -\frac{20ck}{45\mathcal{H}\tau'}\Theta_1 \tag{39g}$$
$$\Theta_l = -\frac{l}{2l+1}\frac{ck}{\mathcal{H}\tau'}\Theta_{l-1} \tag{39h}$$

3.2. Implementation details

We began by implementing logarithmically spaced values for $k \in [5 \cdot 10^{-5}, 0.3]$/Mpc. Then we solved the tight coupling (TC) system with the given initial conditions. The chosen number of multipoles in this section was $l_{\max} = 7$. For the TC system we included all the Θ_l but only explicitly evolved the monopole and dipole as explained in the theory section. However we still implicitly updated the values for $l \geq 2$ with the equations for their initial conditions supplied by the new values for Θ_0 and Θ_1 which recursively affects larger l. If any of the following conditions are true we then exit out of the TC regime:

$$|\tau'| < 10, \qquad |\tau'| < 10\frac{ck}{\mathcal{H}}, \qquad x > -8.3.$$

The necessity of requiring that $|\tau'|$ is relatively low can be seen from (32a). The particular value of τ' to exit the TC regime is not of particularly high importance, and some check with larger τ' values were done to verify this. The next condition comes from imposing different TC regimes at different scales. A proper justification for this can be found in [9]. The final condition is a balance between speed and change in data. Ideally one would want to exit TC as soon as possible, but it turns out that we can keep going for quite some time without any noticeable effects, massively speeding up the computation times.

Once one of these conditions are satisfied, we saved the time in which this occurred, and began to solve the full system. The initial conditions for the full system were supplied by the final values for the TC solution. The solutions are then splined and converted over to data files to be analyzed in Python. We then chose 3 values for $k = \{0.1, 0.01, 0.001\}$/Mpc which have be chosen to assess large, intermediate and small scales respectively.

For the above mentioned scales we plotted the density and velocity perturbations for both CDM, baryons and photons. Further we made some graphs related to quadrupole moment Θ_2 and the Newtonian potentials Φ and Ψ to be discussed in the next section.

3.3. Results

We will consider the modes previously mentioned $k = \{0.1, 0.01, 0.001\}$/Mpc. Since we are generally interested in when causal physics begins to occur, the time at which $k\eta \sim 1$ is of physical significance. As such TABLE III summarizes the times in which one should expect to see the data be affected by any potential gravitational wells and radiation pressure at the given scales. Note that

TABLE III. x values for when $k\eta \sim 1$ and $k\eta \sim 1/\sqrt{3}$ for the different scales. The latter is used for estimating the particle horizon for photons and baryons following previous discussion regarding their sound horizon.

Mode [Mpc^{-1}]	x_{CDM}	$x_{\gamma,\mathrm{B}}$
$k = 0.1$	-11.0	-11.6
$k = 0.01$	-8.5	-9.1
$k = 0.001$	-5.2	-6.1

when photons and baryons are tightly coupled we expect

them both to follow the radiation domination sound horizon instead of the particle horizon. Here we can already see that the large scales should remain unaffected by the radiation pressure due to recombination already having occurred, and hence the universe is neutral by the time causal physics enters. Note that both of these are just approximations as we only really use $k\eta \sim 1$ to separate the times for when $k\eta \ll 1$ where one should not expect any interactions, and $k\eta \gg 1$ for when one should expect to see them. As we will see later, in general, the casual physics begins to enter before the criteria that $k\eta \gtrsim 1$.

As mentioned in the initial conditions section, we have stripped the scaling from all the various quantities. As such one cannot give any meaning to the exact value of any of the quantities as this has been factored out. However we can still interpret the relative changes in the various quantities over time. In the part of the article we will reintroduce this factor which we have gotten rid of.

3.3.1. Matter overdensity and bulk velocity

We begin by considering how the matter density fluctuations and velocities of CDM and baryons change over time, depicted in FIG. 11. Overdensities for these particles are primarily created by gravity pulling matter together once the particle horizon reaches the given scale. As such, we consider TABLE III for when we expect to see these overdensities begin to grow at the various scales depicted with the colored vertical lines.

One thing to note here is that from (29,30), bringing these differential equations to our time variable x, Fourier transforming and setting $\Phi' = 0$ (which we will see later is a reasonable assumptions at certain times), these equations essentially just sets $v \propto \delta'$ for both baryons and CDM given a slow enough expansion rate. This of course implies that the velocity acts as the time derivative of δ given that the potential Φ does not evolve. This is manifest for certain ranges of x if FIG. 11, with some deviances in the range $-12 < x < -6$.

We see that for smaller scales, both CDM and baryons begin to cluster at $x \approx -12$ and their velocities follow one another with equal velocities until $x \approx -11$. This is contrary to what TABLE III suggests, seemingly implying that acausal clustering has occurred, but a reminder that this criteria is a simplification and as such one does not expect this to be completely accurate. A more accurate indication would require considering the sound horizon at the given time. Prior to this there is no clustering whatsoever due to the horizon being much smaller than the scale. Since this is during the radiation epoch, the velocity of all scales can be seen to increase the same amount. The overdensities then continue follow one another until a critical point at around $x \approx -10$. This corresponds to when the outward pressure from clustering photons, as we are in radiation domination at this time, begin to work as a repulsive mechanism to counteract the gravitational pull. However, CDM still continue to cluster up

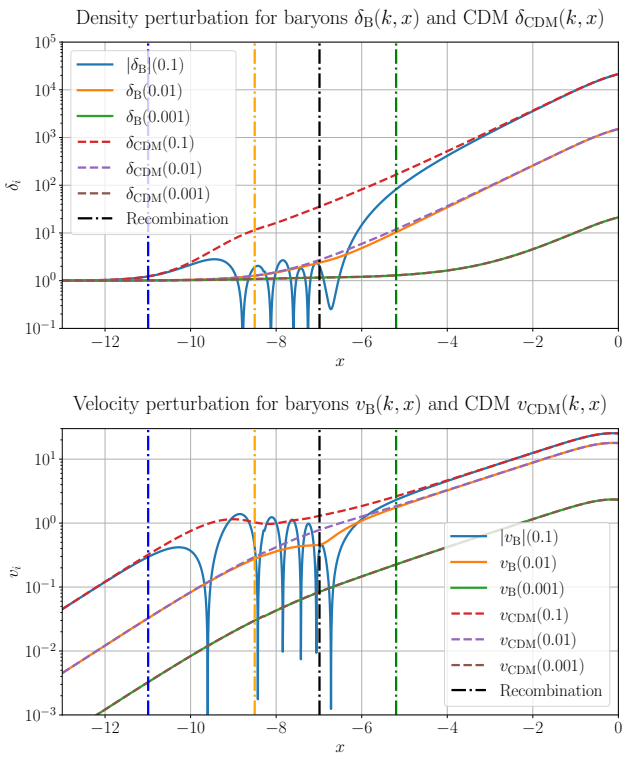

FIG. 11. δ_B, δ_{CDM} and v_B, v_{CDM} as a function of x at modes $k = 0.1$/Mpc, $k = 0.01$/Mpc and $k = 0.001$/Mpc for small, intermediate and large scales respectively. The dot-dashed blue, yellow and green lines correspond to horizon crossing for the small, intermediate and large scale modes respectively.

as they are singlets under electromagnetism and continue to create increasingly deep gravitational wells.

At $x \approx -9$ we can see that there is an equilibrium between the gravitational pull and the outwards pressure from photons. As the gravitational wells from CDM grow deeper, the baryons are pulled back again, creating the oscillatory pattern we see here. We note that is it the absolute value of δ_B and v_B which is being plotted such that it fits on a logarithmic plot. Hence, each dip corresponds to the time where δ_B and v_B switch signs, changing from an overdensity to a lack of overdensity. Reminder that the plots are the Fourier transform of the various quantities. As such the harmonic behavior we see here corresponds to propagating waves of matter density in real space. During this time we can see that this in fact does have an effect on CDM. There is a noticeable drop in their velocity as they begin to follow the baryons due to their gravitational interactions. The counterplay between the combined gravitational pull from matter and the outwards radiation pressure then proceed to play a role for quite some time until recombination occurs. Before this however, one sees that the velocity growth begins to change its power law as we enter matter domination. This causes the universe to accelerate faster, causing velocities to increase at a slower pace. Later, as

the number of free electrons in the universe rapidly decay, the outward pressure from the photons effectively ceases as recombination is in the process of occurring.

The universe then becomes electrically neutral once atoms begin to form, allowing photons to freely travel and no longer impose the outward pressure. This in turn causes the overdensities to begin to grow unbounded from here until they eventually get caught by the gravitational wells caused by CDM. These gravitational wells then begin to snowball and scale exponentially w.r.t. x. This continues until dark energy slows down the overdensity and velocity growth as the exponential growth slightly flattens as the universe begins to accelerate. This effect can be seen on all scales.

For the intermediate scale we can see that there is no overdensity in the graph until about $x \approx -9$ and their velocities remain the same until roughly $x \approx -8.5$. Once again checking TABLE III, there is a reasonable agreement between the plot and the expected time for casual physics to enter. As with the smaller scale, the gravitational pull of CDM and baryons begin to form overdensities. It then comes to a point where the difference between the two become visible at $x \approx -7.5$. Again this is due to the outward repulsion of photons, but to a much smaller extent as the scale is too large for the radiation pressure to have a large effect. At this point the number of free electrons is also relatively low, causing photons to not interact as often. Due to there not being much time until recombination, these oscillations do not have time to manifest, causing the repulsions to stop and thus only allowing for a singular small oscillation. As with the small scale, the baryons begin to form overdensities together with CDM until they once again coincide at a later time.

At the largest scale which we consider one can see that there is in fact no oscillations whatsoever. This was already expected from the previous discussion under TABLE III due to the universe being electrically neutral. Hence one does not expect to see any oscillations whatsoever at these scales and, from this point of view, the baryons simply act as CDM throughout.

3.3.2. Photon overdensity and bulk velocity

We present the photon overdensity and velocity for all the modes we are considering in FIG. 12. As mentioned previously we have the relations between the monopole and dipole and the photon overdensity and bulk velocity respectively: $\delta_\gamma = 4\Theta_0$ and $v_\gamma = -3\Theta_1$. The first of these relations can be justified physically as the photon monopole is a measure of the average photon temperature, which can be related to photon overdensities. A derivation for the factor of 4 can be found in [1]. The latter can be compared to the observation of the CMB spectra as one would see from a non-comoving observer. If one has a velocity w.r.t. the CMB one would see a strong dipole moment depending on the velocity of said observer. As such it is not hard to make the justification that the dipole moment should be related to the velocity. [But finding out why exactly a factor of -3 is correct is not something which I can seem to find a proper argument for.]

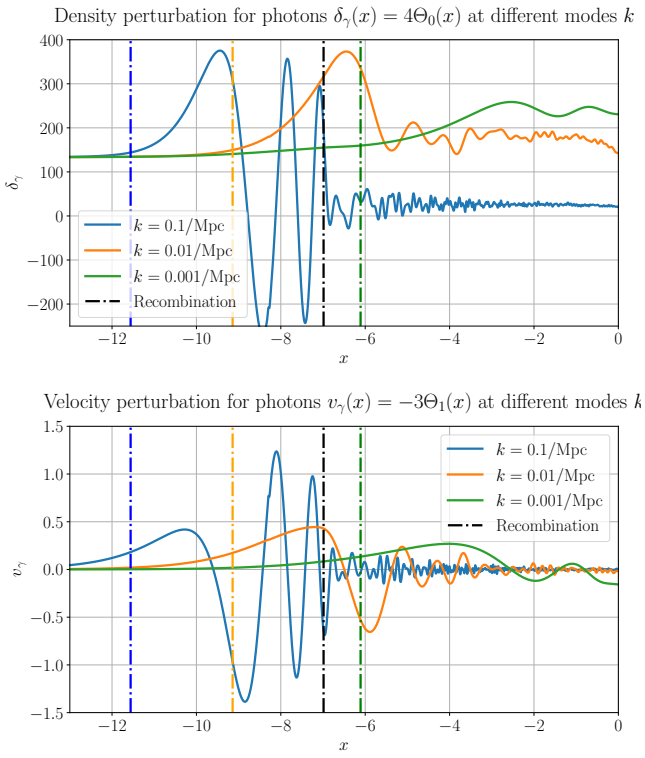

FIG. 12. δ_γ and v_γ as a function of x at modes $k = 0.1$/Mpc, $k = 0.01$/Mpc and $k = 0.001$/Mpc for small, intermediate and large scales respectively. The dot-dashed blue, yellow and green lines correspond to horizon crossing for the small, intermediate and large scale modes respectively and the black dot-dashed line corresponds to the time of recombination.

To gain a clearer understanding of the correlation between the overdensity and velocity of photons and baryons, FIG 13, 14, 15 show δ_γ and v_γ compared to the quantities δ_B and v_B for the modes $k = \{0.1, 0.01, 0.001\}$/Mpc respectively.

As expected from the discussion of the tight coupling regime, the two quantities are deeply related at all scales. Here one sees that even past the tight coupling regime, the two continue to follow one another at all scales, however the overdensities formed by the photons is noticeable larger at all scales. This can be seen from (39) as we begin with $\delta_\gamma = 4\Theta_0 = -2\Psi$, and $\delta_B = -\frac{3}{2}\Psi$ the ratio $\delta_\gamma/\delta_B = 4/3$ exactly as we see in the figure at early times.

For the smallest scale in depicted in FIG. 13 one sees that after horizon crossing, the densities for both photons and baryons begin to grow due to gravitational wells. Later this reaches a peak as the radiation pressure causes an unstable equilibrium at around $x \approx -9.5$. This ra-

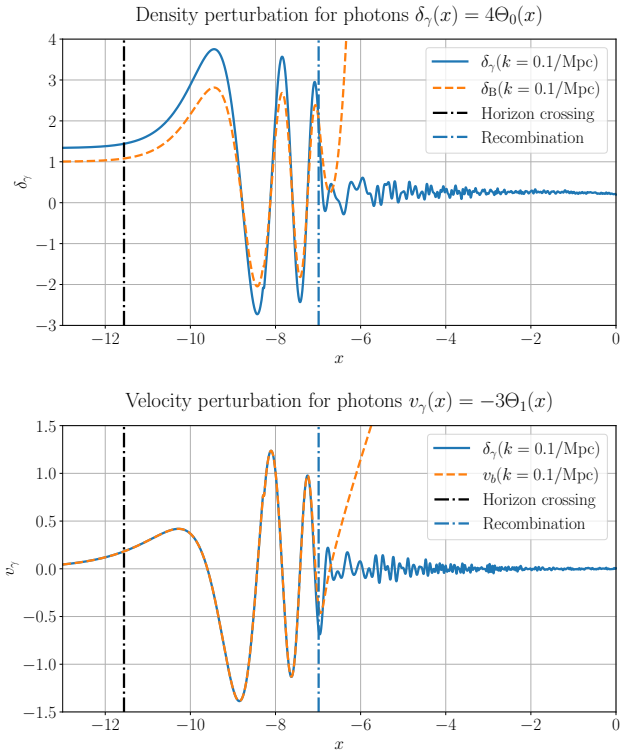

FIG. 13. δ_γ and v_γ as a function of x compared to δ_B and v_B at the mode $k = 0.1/\text{Mpc}$.

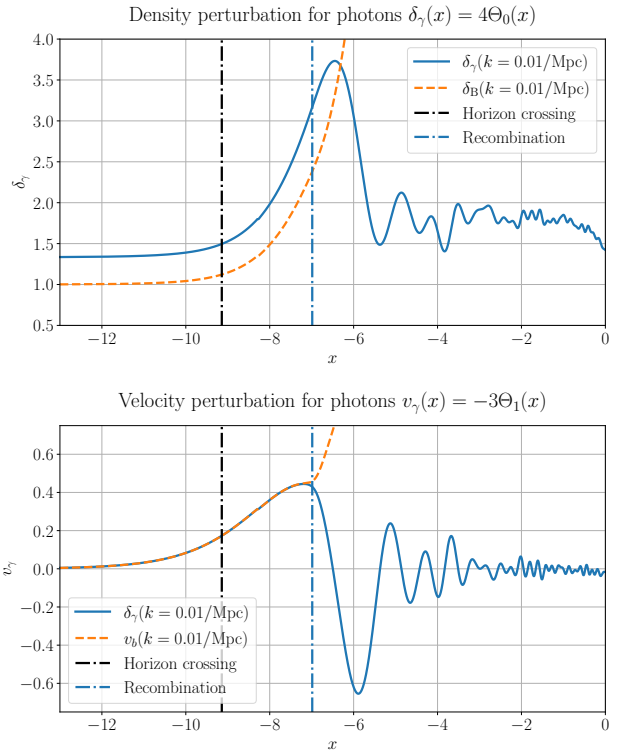

FIG. 14. δ_γ and v_γ as a function of x compared to δ_B and v_B at the mode $k = 0.01/\text{Mpc}$.

diation pressure then drags the baryons along with the photons causing a propagation of the overdensity in the real space. At $x \approx -8.5$ the radiation pressure begins to be dominated by the gravitational wells caused by dark matter as previously discussed. This then occurs a couple more times before recombination occurs. Once this happens, a near instantaneous decoupling between the photons and baryons can be seen, and baryons are left to freely cluster in the ever-growing gravitational wells. From here on the photons are effectively free as neutral atoms form and only experience mild oscillations about the average density fluctuations which we can clearly see is not at 0. Note that the effective photon temperature perturbation is in fact $\Theta_{\text{eff}} = \Theta_0 + \Psi$ [1]. As such one does not expect the oscillations to oscillate about 0 on these scales, but instead that Θ_{eff} does.

In the intermediate scale shown in FIG. 14 we again see much of the same physics as for the smallest scale. As in the discussion for the baryons and CDM, the clustering begins to manifest shortly before the horizon crossing. Here one can more readily see that the clustering occurs until a bit after recombination, but does not have time to cause the oscillatory motion for the baryons that we saw on the smaller scales. The photon density then dips down again until it reaches its equilibrium. Here however one can note that when the universe begins to accelerate, a noticeable second dip in the photon density occurs. This is once again due to dark energy domination occurring and is more prominent on larger scales.

The largest scale that we consider in FIG. 15 the build-up starts much later. Unlike the prior two scales, the velocities of the baryons and photons do not immediately decouple to the same extent after recombination at these scales. But we can still see that there is a noticeable difference in the two past this point. The oscillations in Fourier space after the photon density peak is then much slower here compared to the previous cases due to the propagating waves travelling at velocity $\sim c$ in real space moving much slower relative to the size of the scale.

Next we consider the evolution of the quadrupole moment Θ_2 for the considered length scales depicted in FIG. 16.

One thing to note is that in the derivation of the TC system, an assumption that the early universe is without anisotropic stress, meaning that the stress energy tensor is invariant under spatial rotations. As a consequence, given our conventions, the EFE sets $\Phi = -\Psi$. In the full system this is however not necessarily the case. With this in mind, considering (34b), we see that in this model, anisotropic stress in then deeply related to both Ω_γ and Θ_2. In the era where $\Theta_2 = 0$ we will then expect the sum $\Phi + \Psi = 0$ which we will come back to later.

For the smallest scale we see that the oscillations in Fourier space begin quite late in comparison to when one would expect to see effects due to the horizon crossing. A small oscillation can then be seen to build up rather

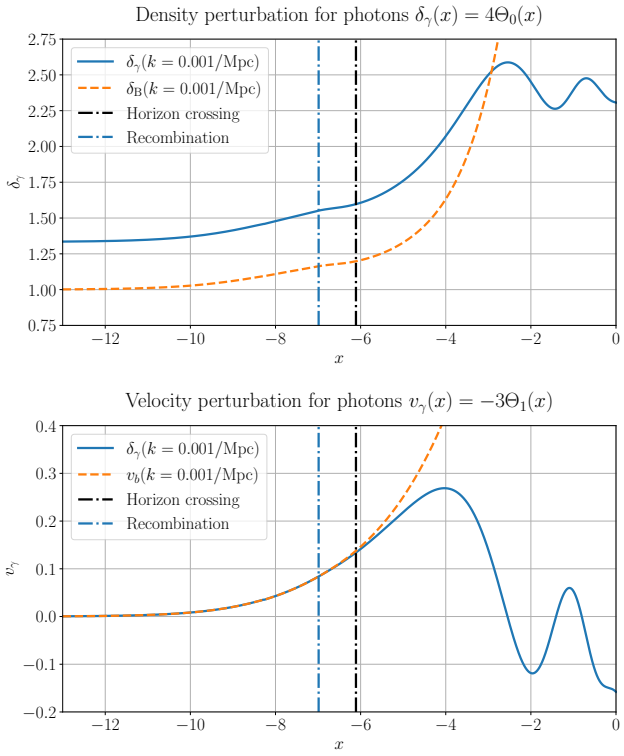

FIG. 15. δ_γ and v_γ as a function of x compared to δ_B and v_B at the mode $k = 0.001/\text{Mpc}$.

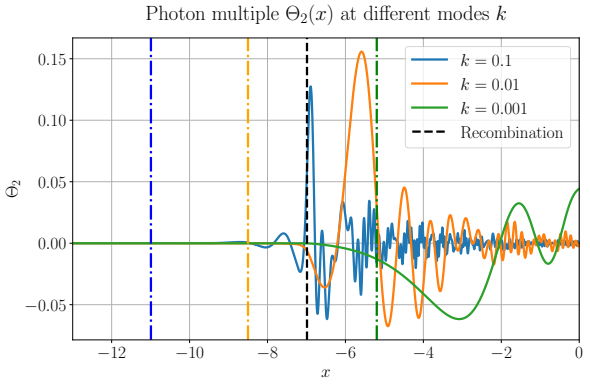

FIG. 16. Time evolution of the photon quadrupole Θ_2 at modes $k = 0.1/\text{Mpc}$, $k = 0.01/\text{Mpc}$ and $k = 0.001/\text{Mpc}$ for small, intermediate and large scales respectively. The dot-dashed blue, yellow and green lines correspond to horizon crossing for the small, intermediate and large scale modes respectively.

quickly until it peaks shortly after recombination. As such the anisotropy that one would expect from photons in the CMB spectra should be rather large at these scales. This also implies that the assumption that $\Phi = -\Psi$ is very poor at this time, something that we will see later. The oscillations then quickly fall off as time evolves past recombination, but are still noticeable compared to before TC ends.

For the intermediate scale we see that the oscillations begin much faster when compared to the particle horizon. As in the small scale the oscillations quickly build up, peaking at about $x \approx -5.5$. This once again signifies a poor approximation of $\Phi = -\Psi$. As with the small scales, the oscillation decay, but albeit at a much slower pace.

At the largest scale we see that the main oscillation starts up before the expected horizon crossing. It then has its absolute extremum at $x \approx -3.5$ and continues its oscillatory motion until present day.

3.3.3. *Gravitational potentials*

Considering the potentials Φ and Ψ as a function of time for the modes $k = \{0.1, 0.01, 0.001\}/\text{Mpc}$ shown in FIG. 17 where the potential Φ is given in the top graph and the sum $\Phi + \Psi$ is given in the lower figure.

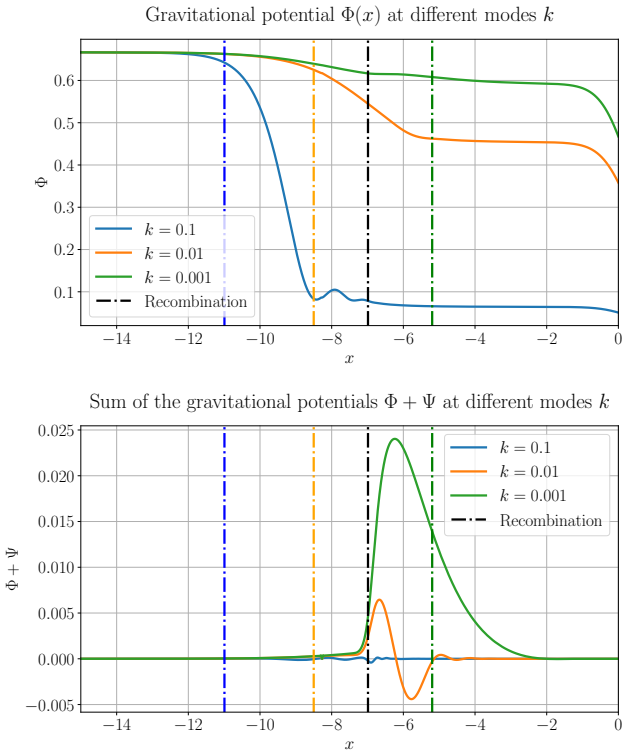

FIG. 17. Time evolution of $\Phi(x)$ along with the sum $\Phi(x) + \Psi(x)$ at modes $k = 0.1/\text{Mpc}$, $k = 0.01/\text{Mpc}$ and $k = 0.001/\text{Mpc}$ for small, intermediate and large scales respectively. The dot-dashed blue, yellow and green lines correspond to horizon crossing for the small, intermediate and large scale modes respectively.

At early times we see that the potential Φ, and thus the potential Ψ are constant as expected due to the horizon being much smaller than the considered modes. As can be seen from the second figure, $\Phi = -\Psi$ at early times

justified by the fact that the quadrupole moment $\Theta_2 = 0$ at this time.

At later times, as the particle horizon expands, the smaller scales, corresponding to the higher value of the modes, enter the horizon. As indicated in TABLE III for small scales, it is expected that causal physics will begin to play a role at around $x \approx -11.0$. In turn this allows for radiation pressure, which is dominant at this time, to effectively counteract the gravitational potential and prevents over-densities to form in the primordial baryon-photon plasma. After a large drop in Φ, it then begins to oscillate in a damped fashion which comes from the back-and-forth between radiation pressure and induced gravitational wells from CDM and baryons. This is clearly seen at smaller scales but the effect is massively suppressed at larger scales. One can also notice that the sum $\Phi + \Psi$ barely changes at these small scales, suggesting that the anisotropies at these scales relatively small, but there are still some small oscillations around recombination as could be expected from FIG. 16. Finally the potential Φ flattens out during matter domination, which is to be expected for $k \gtrsim 0.1/\text{Mpc}$ which agrees with out result.

For the intermediate scales we see that the drop-off of the potential starts later, once again expected from TABLE III and is much slower compared to smaller scales. The drop-off then remains constant with respect to x during recombination until, as before, it flattens out to a constant during matter domination and the anisotropies, in the lower figure, are noticeable at these scales.

The large scale mode begins to drop at roughly the same time as intermediate scales, but once again slower than the others. TABLE III seems to imply that this cannot causally happen at this time. Analytically one can find the expected change to the potential to be a factor of 9/10 as the universe transitions from radiation to matter domination [1] which seems to agree with the green line in the top figure. Further there is a much larger relative difference between the two potentials, due to the k^{-2} dependence in the anisotropy term.

For all scales we see that during matter domination, the gravitational potentials flatten out at every scale. Naively one would expect it to increase in this period as all matter is effectively neutral and thus things would collapse together gravitationally, but the expansion of the universe works as a counteractive force against gravitational wells, and thus it remains roughly constant at all scales. In the lower figure we see that at late times the sum of the Newtonian scalars once again satisfy $\Phi = -\Psi$. Again referring (34b) we have that $\Omega_\gamma \approx 0$ past a certain point. As such, even with the continuing oscillatory motion of the quadrupole moment, the anisotropies are cancelled out by the lack of radiation at late times. At last one sees a drop-off, where the magnitude of this drop-off is seemingly proportional to the scale, as the universe begins to expand due to dark energy beginning to dominate. This makes sense physically as when the repulsive nature of dark energy takes over, it will expand the distance between massive objects, causing the gravitational potentials to fall off.

3.4. Summary

In this section we first solved the approximated tight coupling system and exited this system before our approximations broke down. We then switched over to the full system up to the given $l_{\max} = 7$. Three particular modes, each representing a given scale, were then chosen and discussed for the various quantities.

[I will make more proper summaries at a later time for all the milestones and move all conclusions to the end of the entire paper into a combined conclusion once milestone IV has been finished. As such no conclusion for this one.]

4. MILESTONE IV

Some introduction about what it is all about.

4.1. Theory

The theory behind this milestone.

4.2. Implementation details

Something about the numerical work.

4.3. Results

Show and discuss the results.

ACKNOWLEDGMENTS

...

[1] H. A. Winther, H. K. Eriksen, O. Elgaroy, D. F. Mota, and H. Ihle, "Cosmology ii." `https://cmb.wintherscoming.no/`, 2023. Accessed on March 1, 2023.

[2] Planck: N. Aghanim *et. al.*, *Planck 2018 results. VI. Cosmological parameters*, *Astron. Astrophys.* **641** (2020) A6, [`arXiv:1807.06209`]. [Erratum: Astron.Astrophys. 652, C4 (2021)].

[3] SDSS: M. Betoule *et. al.*, *Improved cosmological constraints from a joint analysis of the SDSS-II and SNLS supernova samples*, *Astron. Astrophys.* **568** (2014) A22, [arXiv:1401.4064].

[4] S. Dodelson, *Modern Cosmology*. Academic Press, Amsterdam, 2003.

[5] T. M. Davis and C. H. Lineweaver, *Expanding confusion: Common misconceptions of cosmological horizons and the superluminal expansion of the universe*, *Publications of the Astronomical Society of Australia* **21** (2004) 97–109.

[6] J. R. Gott, III, M. Juric, *et. al.*, *A map of the universe*, *Astrophys. J.* **624** (2005) 463, [astro-ph/0310571].

[7] E. Di Valentino, O. Mena, *et. al.*, *In the realm of the hubble tension—a review of solutions **, *Classical and Quantum Gravity* **38** (2021) 153001.

[8] S. M. Carroll, *Spacetime and Geometry: An Introduction to General Relativity*. Cambridge University Press, 2019.

[9] M. Doran, *Speeding up cosmological Boltzmann codes*, *JCAP* **06** (2005) 011, [astro-ph/0503277].